Accepted Manuscript

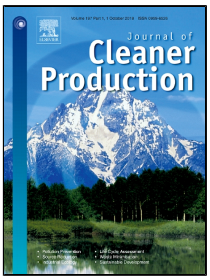

Microstructure and engineering properties of Fe_2O_3(FeO)-Al_2O_3-SiO_2 based geopolymer composites

Rodrigue Cyriaque Kaze, Lynn Myllyam Beleuk à Moungam, Maria Cannio, Roberto Rosa, Elie Kamseu, Uphie Chinje Melo, Cristina Leonelli

PII:	S0959-6526(18)32160-7
DOI:	10.1016/j.jclepro.2018.07.171
Reference:	JCLP 13625
To appear in:	*Journal of Cleaner Production*
Received Date:	14 November 2017
Accepted Date:	16 July 2018

Please cite this article as: Rodrigue Cyriaque Kaze, Lynn Myllyam Beleuk à Moungam, Maria Cannio, Roberto Rosa, Elie Kamseu, Uphie Chinje Melo, Cristina Leonelli, Microstructure and engineering properties of Fe_2O_3(FeO)-Al_2O_3-SiO_2 based geopolymer composites, *Journal of Cleaner Production* (2018), doi: 10.1016/j.jclepro.2018.07.171

Microstructure and engineering properties of $Fe_2O_3(FeO)$-Al_2O_3-SiO_2 based geopolymer composites

Rodrigue Cyriaque Kaze[a,*], Lynn Myllyam Beleuk à Moungam[b], Maria Cannio[c], Roberto Rosa[c], Elie Kamseu[b,c**], Uphie Chinje Melo[a], Cristina Leonelli[c]

[a]Laboratory of Applied Inorganic Chemistry, Faculty of Science, University of Yaoundé I, P.O. Box 812, Yaoundé, Cameroon.

[b]Laboratory of Materials, Local Materials Promotion Authority, MINRESI/MIPROMALO, P.O. Box 2396, Yaoundé, Cameroon.

[c]Department of Engineering Enzo Ferrari, University of Modena and Reggio Emilia, Via Vignolese 905/A, 41125 Modena, Italy

*Corresponding author: Tel. 00237673259397; e-mail: cyriaque.kaze@uy1.uninet.cm kazerodrigue@gmail.com (R. C. Kaze)

**Author to whom further correspondence should be addressed: Tel: 00237222229445; Fax: 00237222223720; e-mail: kamseuelie2001@yahoo.fr (E. Kamseu)

ABSTRACT

The objective of this study is to develop low cost, eco-friendly and sustainable building materials by applying the technology of mineral polymerization (geopolymerization) process on naturally abundant iron-rich aluminosilicate (laterite) materials. Iron-rich aluminosilicates based-geopolymer composites containing 10 to 40wt% of rice husk ash (RHA) were cured at room temperature and at 90 °C. This paper examines the phase transformation, microstructural and mechanical changes that occur in the geopolymer composites when fine aggregates of quartz sand are added. Experimental results indicate good polycondensation and more cohesion resulting in high strength due to the better dissolution of RHA that provides soluble reactive silica to equilibrate the Si/Al and Si/Fe molar ratios. Ferro-sialates, Fe(Al)–S–H, were identified at the room temperature in addition to polysialates, S–A-N–H, phases. The flexural strength of resultant composites increases from 10–12 MPa for room temperature curing to ~ 40 MPa when the composites were cured at about 90 °C as from the intensive formation of ferrisilicates. The formation of ferri-silicates that changed the flexural strength and microstructure seem to play significant role in the engineering properties of laterites based geopolymer composites making them promising candidates for applications as pavements, roads and building construction.

Keywords: laterite, rice husk ash (RHA), geopolymerization, ferri-silicate, mechanical strength, microstructure

1 Introduction

Laterites and lateritic soils, described as $Fe_2O_3(FeO)–Al_2O_3–SiO_2–H_2O$ matrices, are made from kaolinite in which a high proportion of Al^{3+} is replaced by Fe^{2+} or Fe^{3+} (Lyon Associates, Inc., 1971; Kamseu et al. 2013; Obonyo et al. 2014). These materials are available in tropical and sub-tropical areas of the world, with nearly 67% found in the Cameroonian territory (Mbumbia et al. 2000). The replacement of aluminium by iron atoms in kaolinite structure affects their crystallinity with consequent increase of amorphous content and enhance their vulnerability to chemical attack (Obonyo et al. 2014; Pignatelli et al. 2014; Kaze et al. 2017). Geopolymers produce from natural iron-rich aluminosilicate (laterites) without treatment should be eco-friendly and more greener in comparison of metakaolin based geopolymer which requires an energy for the thermal treatment in the range of 700-800 °C (Kamseu et al. 2011; Elimbi et al. 2011, Kamseu et al. 2014, Tchakoute et al. 2016). The use of laterites as raw materials for the development of geopolymers might be considered as the way for the reduction of amount of CO_2 emitted from cement industries and also the energy used to activate the clay materials. As reported by Kamseu et al. (2013) and Obonyo et al. (2014), it is easier in tropical areas to have laterites, generally at the surface, than struggle for clays for which exploitation will be detrimental for the environment because they are covered in most cases by laterites or various types of soils. Therefore a sustainable materials from activated laterites locally sourced, with negligible transport costs and environmental impact, will present thermal efficiency, financial viability and low energy required in the manufacturing process as mentioned by Duxson et al. (2007).

This paper is the second in a series of articles describing the use of laterite for the development of geopolymer composites. It explores the engineering properties of two laterites, with similar degree of laterisation (~35wt% of $FeO(Fe_2O_3)$ used for the preparation of alkali activated materials, hereafter indicated as geopolymer composites, with addition of rice husk ash under different curing conditions.

Physical and chemical properties of laterites based geopolymers were described in the first paper (Kaze et al. 2017). We observed that, the values of flexural strength of laterites based geopolymers are similar to those of standard metakaolin based geopolymers and decrease with the thermal activation of solid precursors above 500 °C (Kaze et al. 2017). The setting

time and the water absorption also decreased with thermal treatment of laterite. Their microstructure appeared coarse and more inhomogeneous with the increase of the calcined temperature above 500 °C. In recent times these soils were valorised as potential candidate for the development of geopolymer cements (Cristiane et al. 2010; Kamseu et al. 2013; Obonyo et al. 2014; Lemougna et al. 2014; Lassinantti et al. 2015; Nik Ab Aziz et al. 2015; Kaze et al. 2017) while others preferred mixtures with cement (Jayasinghe and Mallawaarachchi 2009). The most used of traditional precursor materials for geopolymers are like metakaolinite (Fe_2O_3 content of 2-5%), fly ash (Fe_2O_3 content of 10%), volcanic scoria (10-15%) and blast furnace slag (Fe_2O_3 content of 0.5%). Nevertheless, recent studies have shown that precursors with iron content higher than the usually found in fly ashes and volcanic scoria may be activated in alkaline environment (Kaze et al. 2017; Gomez et al. 2010; Kamseu et al. 2013; Obonyo et al. 2014; Lemougna et al. 2014) with potential applications in engineering. Gomes et al. (2007) observed that, the alkaline activation of raw material with high iron and low aluminium content produced the geopolymer with compressive strength ranging from 20 to 80 MPa. Obonyo et al. (2014) reported that the addition of calcined low iron content laterite (up to 30% mass) to poorly reactive natural laterite in alkaline medium, led to geopolymers with improved 28 days physical and mechanical properties. The detailed microstructure of products of the geopolymerization of laterites revealed low level of homogeneity and phase distribution although the relative good mechanical strength in comparison with standard geopolymer cements. The presence of some large capillary pores also affect the final properties of products of geopolymerization of laterites. In our point of view the poor homogeneity and larger and non-homogeneous porosity are due to alumina and iron-rich oligomers that remain unbounded to the geopolymer system after geopolymerization. This study aims to investigate the possibility of using rice husk ash (RHA) as SiO_2 source for the improvement of the strength and stability of Fe_2O_3(FeO)-Al_2O_3-SiO_2 systems, sustainable inorganic polymers materials (geopolymers). We plan the experimental design so that sufficient amount of soluble silica added to the laterite-based geopolymer composites will combine all the residual Al and Fe-oligomers that do not react effectively in laterites. The soluble silica provides Si-based oligomers to develop more bending phases. The three-point flexural strength was used as an indicator for the bending bonds development. The microstructural analysis of geopolymer composites was done through Environment Scanning Electron Microscope (ESEM) analysis to understand the features of the composites. The Mercury Intrusion Porosity (MIP) and water absorption were also studied to evaluate and

appreciate the pore sizes distribution within specimens. The main factors that govern our investigations include percentages of RHA (SiO_2 source) and curing process.

2 Materials and Experimental methods

2.1 Materials and characterization

The iron-rich aluminosilicates (laterites), LATOD and LATEL, used in this study were extracted respectively at laterite deposit of Odza and Eloumden (Yaoundé town, Central Region of Cameroon). These materials are currently used in roads construction by the enterprise RAZEL Cameroon, Yaoundé, Cameroon as in earth fill dam and highway. The dried raw materials were ground with a grinder (model BULLI I. PIAMO, M.M.S., Modena, Italy) for 4 hours (rpm = 1200) in order to have fine powders with particles down to 80 µm. The chemical composition of both laterites carried out by X-Ray Fluorescence analysis (Thermo ARL, ARL Advant XP and XP^+ X-Ray Fluorescence Spectrometer, Thermo Fisher Scientific, MA, USA) using argon-methane as inert gas is reported in Table 1. The concentration is given in wt% or ppm by the data Quanta As modelling software. The mineralogical composition of both laterites were determined by X-ray powder diffraction (XRD) analysis (PANAlytical X'Pert PRO diffractometer, Ni filtered Cu-Kα radiation, λ = 1.5405 Å). Both laterites present the similar mineral phases (kaolinite, quartz, goethite, anatase, rutile, hematite, maghemite and ilmenite), except lepidocrocite contained in Eloumden's laterite (see Figure 1). The particle size and B.E.T. surface area were determined by Kaze et al. (2017). The average values of the particle sizes $d_{0.5}$ were 34.90 and 38.30 µm for Eloumden and Odza, respectively, those of $d_{0.1}$ and $d_{0.9}$ were: 2.48 and 3.39 µm for Eloumden; 106.20 and 170.70 µm for Odza. The B.E.T. surface are 21.92 ± 0.11 m^2/g and 23.87 ± 0.13 m^2/g for Eloumden and Odza, respectively (Table 2).

Rice husk was collected from Ndop, Department of Ngoketundjia, Region of North-West (Cameroon). The silica source (RHA) was obtained from calcination of dried rice husk at 600 °C for 2 h (heating/cooling rate of 5 °C/min). The chemical composition of RHA is presented in Table 1, and its XRD pattern (Figure 2) shows a typical broad hump diffraction peak in the range between 2θ = 15° and 35° with maximum around 21°, which implies the high amount of amorphous phase of silica from calcined rice husk (Tchakouté et al. 2016). Some quartz peaks were also observed.

The NaOH solution was prepared by dissolving laboratory grade granules (98 wt%, Sigma Aldrich, Italy) into distilled water to have 8 M concentration. The commercial sodium silicate solution (SiO_2/Na_2O = 3.00; loss of ignition = 60 wt%) was provided by Ingessil S.r.l., Verona, Italy.

2.2 Geopolymer synthesis

Alkaline solution used in this study was prepared by a mixture of 8 M NaOH and the commercial sodium silicate solution in the volume proportion 1:1. For each 100g of laterite, 10, 20, 30 and 40 g of RHA were added. The mix composite was dried, homogenized for 5 min and received the alkaline solution in the proportion solid/liquid of ~ 1-6. Finally the river sand (sand was collected from Sanaga river with particles size between 2.0 - 0.075 [AASHTO]; specific gravity and fineness modulus of 2.38) was added with a proportion paste: sand of 1:2 and homogeneous paste was obtained by ball-milling. The pastes were poured into plastic moulds with dimensions 1×1×14 cm^3 at room temperature (23±3 °C; RH 55%) for 3 h, then oven cured at temperatures of 90 °C for 24 h. Curing at room temperature with ambient conditions was also applied for comparison. The geopolymer samples were left for 28 days at ambient temperature prior to three-point flexural strength testing. The geopolymers specimens were labelled as GPEL, GPOD for the as received and ground laterites from Eloumden and Odza. Materials obtained with addition of RHA were labelled: GPEL10, GPEL20, GPEL30, GPEL40, GPOD10, GPOD20, GPOD30 and GPOD40 as in Table 3.

2.3 Characterization methods

2.3.1 Physico – chemical tests

Three-point flexural strength of the samples was measured with an Instron® 1195 compression machine with a displacement of 5 mm/min. The results shown are an average of five to six replicate specimens. The strength is given by the equation (1):

$$\sigma = \frac{3\,F\,L}{2\,b\,h^2} \qquad (1)$$

where σ is the maximum center tensile stress (MPa), F maximum load at fracture (N), L the distance between the supports (mm), b the width and h the thickness of the specimen (mm).

The three-point bending strength tests were performed according to the standard test method for flexural strength of concretes ASTM C78-16.

The water absorption analysis was carry out by immersing the specimen in water at ambient temperature for 24 h and comparing the humid weight (*mh*) to the dry weight (*md*) according to equation (2):

$$Wa = \frac{(mh - md)}{md} x\ 100 \qquad (2)$$

2.3.1 Microstructural characterization and phase's analysis of geopolymer composites

The microstructure of the inorganic polymer cement specimens was studied using an Environmental Scanning Electron Microscope (ESEM, Model Quanta 200, FEI, and Hillsboro, OR, USA) at low vacuum. Both fractured pieces from mechanical test and etched polished specimens were used. The specimens were preliminarily coated with 10 nm thick gold layer.

Pieces collected from the mechanical test were used to prepare specimens of ~1 cm^3 of volume for the Mercury Intrusion Porosimeter (MIP) (Autopore IV 9500, 33000) tests using psia (228 MPa) MIP covering the pore diameter range from approximately 20–0.001 µm having two low-pressure ports and one high-pressure chamber.

The mineralogical phases of resulting geopolymers were identified via X-ray powder diffractometer, XRD, as described above.

Fourier Transformed Infrared Spectroscopy, FTIR, (VERTEX-70 FTIR, Bruker, Ettlingen, Germany) was performed on selected sample analyzing fine powder of ground specimens ($\phi \leq$ 80 µm) collected from pieces of the mechanical test cured at 28 days. A minimum of 32 scans between 4000 and 500 cm^{-1} were averaged for each spectrum at intervals of 1 cm^{-1}.

3. Results

3.1 Microstructure

3.1.1 Effect of amorphous silica (RHA)

The geopolymerization products of laterite (35% $FeO(Fe_2O_3)$) have shown the flexural strength in the range of 4-6 MPa, with water absorption less than 13% and similar to the characteristic properties of metakaolin based geopolymer (Kaze et al. 2017). Despite these properties, the microstructure of laterite based geopolymer exhibited more cracks, large pores, with the poor distribution of grains into the matrix (Figure 3). The thermal treatment of

starting materials at temperature >500°C (600 and 700 °C) does not exhibited a coherent, compact and homogeneous microstructure. These temperatures induced more microcracks within geopolymer matrix. The presence of Fe ions contribute to the reduction of the Si/Al molar ratio making available Al and Fe oligomers lossely bounded into the matrix. In fact, in the geopolymers, Si^{4+} and Al^{3+} are the network formers and inhomogeneity and microcracks came from the lack of stoichiometry equilibrium of these ions. The micrographs of Figures 4 and 5 let observe microporous microstructure of laterites based geopolymer composites with addition of RHA with more homogeneity and coherence; the quartz grain are not visible. The geopolymer composite can be described as amorphous to semi-crystalline mass in which are embebded the residual crystalline grains of quartz sand. This definition is more significant when 30-40 wt% of amorphous silica (RHA) is added. Further investigation with EDS (Figure 6) showed that, at this level, the iron phases are distributed homogeneously into the matrix. The surface fractures give the impression that the composite possess a high fraction of amorphous mass as described by Gallup (Gallup 1989). In fact, he described the iron silicate as brownish and blackish solid "vitreous mass", generally formed at T≤ 200 °C with composition; 48.98 (Fe); 42.77 (Si) and 12.55 (H_2O). Several Si/Fe ratios were observed into these "vitreous mass" and when the temperature increases (50-200 °C), the iron silicates (ferri and ferrosilicates) content is raised. According to Quong (1976), the iron silicate does not exhibit an X-ray diffraction pattern and therefore it has been considered as an amorphous mass. In general, the amorphous mass has a non-stoichiometric composition with Si/Fe ratio in the range of 0.1-1 (Gallup 1989). The amorphous mass could be ascribed to hydrated silica, with iron being bound to silica through oxygen bridges, like Fe–O–Si structure extended into the matrix of geopolymer composite. This is also confirmed by the large absorption bands observed on FTIR spectra (Figure 7). The micrographs of composites show in the inter pores spaces, a dense and homogeneous interconnected structure similar to that observed for volcanic scoria (Polacci et al. 2008). These observations prove that the present Fe atoms in iron silicate are chemically bounded to silica and cannot consist of a simple mixture of silica and iron oxide within the matrix of geopolymer. Gallup (1989) described the matrix being a SiO_4 groups with random H–O–Si linkages suggesting a three-dimensional polymer of silica containing bounded iron substituting for H in the SiO_4 groups where O-H and O-Fe bonds are located at apices of the tetrahedron.

3.1.2 Effect of temperature and residual humidity

The three-point flexural strength of geopolymer composite cured at room temperature are in the range of 10–12 MPa, with water absorption between 10–13% (Figures 8 and 9). The

addition of 10, 20, 30 and 40 wt% of amorphous silica from biosource, i.e. RHA, favours the formation of a homogeneous microstructure with high compactness, no large pores and microcracks similar to the metakaolin based geopolymer with Si/Al ratio ~ 2-3 (Kamseu et al. 2013; Kamseu et al. 2014). The increase of flexural strength and high compactness/cohesion of microstructure is a good indication of the bonding role played by amorphous silica. In fact, the silica oligomers formed from the dissolution of amorphous silica in alkaline environment allowed the polymerization of the residuals alumina and iron oligomers. Indeed, in the chemical context of laterite based geopolymer, where the reactive silica was added, it appears the simultaneous formation of polysialates and ferrosialates (Davidovits et al. 2012). Figure 4 illustrates the microstructure of geopolymer with amorphous silica (40wt% of RHA) oven cured at 90 °C. The particularity of this microstructure is the homogeneous distribution of micropores (10-30 μm) and a densification of matrix inter pores. As seen from the mechanical properties in Figure 9, it is noted an exponential increasing of strength around 20-40 wt% of RHA added. Practically, 45 MPa of flexural was attained with curing at about 90 °C. The increase of strength between 20-40 wt% of RHA and the particular conditions to obtain the microstructure illustrated in Figures 4-6 confirm the hypothesis of the complex exothermic reaction among silica, iron and humidity, in optimal conditions of reactive silica, relative humidity and temperature. The micropores, homogeneously distributed in final matrix, may be explained by the formation of iron silicate following the dissolution of solid precursors (Fe, Si, Al, Ti etc.) in alkaline medium. During the dissolution, the metallic ions would be corroded, thereby the released gases are responsible for the observed micropores. Similar results were observed as consequence of water evaporation during an oven curing. According to Greenwood and Gibbs (1971), at relatively high temperature (200 °C), iron silicate is present with iron in the ferric (+3) oxidation state with only trace of ferrous (+2) iron. The low temperature (100 °C) is shown to consist of both ferric (46%) and ferrous iron (54%).

In both materials the mineral phases such as lepidocrocite, ilmenite, goethite and hematite are potential mineral sources of ferric and ferrous irons. Ferric irons were detected in the iron-rich (laterite) aluminosilicate using Mössbauer spectroscopy, suggesting a replacement of Al^{3+} by Fe^{3+} in octahedral sites, most likely within the kaolinite phases (Gomez et al. 2010). The Mössbauer spectra analyses indicated that the structure of Fe^{+3} was associated to the crystalline phases: hematite and goethite. Iron silicate is believed to form by the reaction of hydrated ferric oxyhydroxide with mono-silicic acid or silicic acid oligomers as follows:

$$OFeOH \cdot H_2O + Si(OH)_4 \rightarrow Fe(OH)_3.SiO_2 + 2H_2O \quad (1)$$

This scale-forming reaction is believed to occur quite rapidly because ferric iron is known to have a strong affinity for silica (Gallup 1989). In the same time a fraction of kaolinite in raw laterite, under oven curing, is converted to hydrosodalite or sodalite. The kaolinite present in higly corroded laterites is amorphous or metastable (disordered) making it easier to be transformed into polysialates or ferrosialates in alkaline medium (Equation 2).

Si_2O_5, $Al_2(OH)_4$ + NaOH → Na(Si-O-Al-O)n (2)

The action of the temperature affects the porosity and pore-size distribution while the residual humidity is significant for the effectiveness of the dissolution and polycondensation.

3.2 Phases evolution

The infrared spectra of resultant products are presented in Figures 7a-d. The strong bands at 1010–1013 cm^{-1} (Figures 7a-b) and 1007–1012 cm^{-1} (Figures 7c-d) observed in both laterites based geopolymer composites (GPOD and GPEL) are assigned to the stretching of Fe–O–Si bonds. These bands are similar to those obtained previously by Schwertmann and Thalmann (1976); Carlson and Schwertmann (1981), Vempati and Loeppert (1989); Gallup and Reiff (1991), who attributed the bands to Si-O-Fe bonds in Fe-Si hydrous oxides and silicates. While the bands at about 787–846 cm^{-1} were attributed to Fe–O–Al, Fe–O–Fe, Fe–O–Si and Si–O –Si bonds (Moenke 1974; Goodman et al. 1976). Into literature, the bands at 787 – 846 cm^{-1} are known to be linked to the formation of geopolymer gel. The smallest bands at about 690 cm^{-1} in all geopolymer spectra are attributed to Fe-O and Si-O stretching and deformation vibrations (Farrell, 1972; Sidhu, 1988). Those around 1300–1450 cm^{-1} are linked to stretching C-O bonds in all spectra due to the formation of sodium/iron carbonate from reaction of residual alkali metal with CO_2. The last one with lower frequency band at 3240–3280 cm^{-1} appear to be an overtone of the vibration of the silicate framework as already pointed by White and Keester (1965). The bands of Si−O−T (T = Al, Fe or Si) which were in the range of 1015–980 cm^{-1} in previous work (Kaze et al. 2017) are shifted to the high values of wave numbers about 1020 and 1030 cm^{-1} with increase of reactive silica from rice husk ash. This behavior is due to the formation of (Si, Fe and Al) -rich gel. Similar trend was reported by Rees et al. (2007) and Kamseu et al. (2017), which attributed the band positions greater than 995 cm^{-1} to a very high Si content. The high values of wavenumbers also described the presence of fayalite mineral as reported by Hofmeister (1987).

The XRD patterns of raw laterites (LATOD and LATEL) and selected geopolymer composites samples (GPEL20; GPOD20; GPEL40 and GPOD40) treated at about 90 °C are shown in Figures 8a-b. The mineral phases identified into the geopolymer composites are: hematite, quartz, maghemite, anatase, ilmenite, which are also present in raw laterites, suggesting that they were not involved in geopolymerization reaction. It should be noted the decrease of kaolinite reflections after geopolymerization: the decrease confirms the poorly crystallized nature of the kaolinite, the principal mineral of laterite (Kaze et al. 2017). The phase's formation that includes zeolite, hydrosodalite and iron silicate minerals (fayalite, and others) has evolution depending on the curing cycle adopted. At room temperature the products of geopolymerization of laterite is essentially hydrosodalite, while the curing cycle including the treatment between 60-100 °C and controlled humidity produces hydrosodalite, zeolite and fayalite. Peaks characteristics of zeolite A, most notably at ~ 7-8° (2θ), are observed in geopolymer diffractograms particularly most evident when the curing includes a treatment above 50 °C. Sore et al. (2016) studied the mixture of metakaolinite with rice husk ash and collected similar results when considering the geopolymerization: in fact while the reaction at room temperature gave essentially amorphous phases (geopolymer gel) they found that the curing between 60–90 °C promoted zeolite as the predominant crystalline phase. Similar results were described by Davidovidts (1988), Subaer et al.(2004) and Heah et al. (2012). The latter used kaolinite which is more similar to our work. In alkaline medium the goethite mineral is dehyroxylated and then reacts with silicate to form fayalite, which appears at the peaks around 25°, 38.4°, 60.8° (2θ); (fayalite Fe_2SiO_4 PDF, 34-178). The geopolymer composite diffractograms appeared as more crystalline in comparison with the conventional XRD patterns of other aluminosilicates (metakaolin, fly ash) based geopolymers. Thereby the new amorphous phases is drown within crystalline phases, affecting significantly the halo band generally observed with standard metakaolin based geopolymers. The presence of crystalline phases in alkaline medium also contributed to the increase of strength. Partial substitution of laterite by silica biosource (RHA) promoted the formation of amorphous phases, which contributed to a decrease in crystallinity of hydrates formed, marked by less intensity peaks in comparison with XRD diffractograms of raw laterites.

3.3 Flexural strength

The three-point flexural strength increases with the rice ash husk content and curing cycles as summarized in Figure 9. The geopolymer products of laterite without addition gave an average of ~4MPa (Kaze et al. 2017). The addition of 10, 20, 30 and 40 wt% gave respectively 6, 10, 24 and 39 MPa. This behavior is in line with the increase of chemical bonds due to the formation of new phases. According to Obonyo et al. (2014) the strength is function of the amount of geopolymeric gel developed capable to embed the matrix.

From 30-40 wt% of RHA 24.81 and 35.22 MPa (GPOD series), 20.83 and 39 MPa (GPEL series) of flexural strength were achieved respectively indicating the better polycondensation/geopolymerization. Such improvements can be explained by two reasons: (i) an increased amount of reactive silica from the RHA results in a higher density of the Si-O-Al(Fe) bonds in the geopolymer, leading to a higher strength and stiffness; and (ii) at 90 °C, a higher amount of RHA with a high specific surface area makes the end products more ductile. On the other hand the use of RHA as silica source increases the amount fraction of amorphous and then improves the chemical bonds, Si-O-Fe, Si-O-Al and the formation of ferrosialate as well as iron silicate, which allowed dense matrix and re-equilibrates the Si/Fe, Si/Al and Al/Fe ratios during the alkaline activation. By the way increases the gel content that favors the cross-linking of the particles phases. It is important to note that, the curing of specimens in this case maintained at constant temperature of approximately 90 °C enhanced the mechanical properties of the final products. The synergy between the geopolymer phases and the ferro-silicates resulted in a significant improvement of the strength into the matrix although the presence of an important fraction of micropores making the curing at 90 °C ideal for the design of laterites based geopolymer composites.

3.4 Porosity, Pore Size Distribution and Water Absorption

The values of water absorption of geopolymer specimens cured at room temperature and at 90 °C are given in Figure 10. It is seen that the values of water absorption decrease from 14.03 to 8.37% and 16.03 to 9.76% at room temperature respectively for GPOD and GPOL (Figure 10a). When the curing implies treatment at 90 °C, the values of water absorption decrease from 15.89 to 7.40% and 15.03 to 7.89% (Figure 10b). This decrease of water absorption is due to the action of RHA, which favors the connectivity and polycondensation of raw materials, then improves the cohesion between particles and leads to smaller pores occurred into the matrix network. These values are relatively low in comparison with those obtained from metakaolin based geopolymers (Elimbi et al. 2014).

The results of MIP analysis of selected geopolymers (GPEL40 and GPOD40) samples are shown in Figure 11. With the particular microstructure of the laterites based geopolymer composites, the nanometric pores characteristic of the geopolymer gel see their band shifted to lower values with the peak at 0.00452 μm. These nanometric porosities are concentrated into the interpores spaces in which the significant reduction of the pore size can partially explain the level of strength exceptionally high with respect to normal geopolymer. The micrometric porosity resulting from the combined action of the metallic iron and water evaporation during the dissolution/polycondensation and curing forms the second band of the system: 5.76–53.51 μm (Figure 11a). Similar results were noted by Kamseu et al. (2016) on steel slag based geopolymer mortars, where they attributed the increase of fraction of larger capillary pores within samples to the action of metallic iron during the alkaline activation.

The values of the cumulative pore volume are 92.58 and 120.21 mm^3/g, respectively for specimens GPEL40 and GPOD40 (Figure 11a). The larger pore size was observed to be 9 and 60 μm, respectively for GPEL40 and GPOD40. The high value of pore volume observed on GPOD40 samples is linked to the presence of larger porosity with respect to GPEL40. This could be explained by a detailed analysis of ESEM micrographs collected for the different samples at higher magnification (Figures 3-6). These results are in accordance with the trend of mechanical properties. From the difference mentioned above, it is seen that the geopolymers GPEL40 exhibited a more compact structure than GPOD40, which allows a low value of water absorption due to smaller pores radius after an immersion in water. From Figure 11b, the large pores that are randomly dispersed in both geopolymer matrices, and in some cases larger than the range of measurement of the mercury intrusion porosimeter as reported by Kamseu et al. (2013), are linked to bubbles formed during the iron corrosion in alkaline media and water evaporation. These larger pores were not taken in account from MIP evaluation. Then pores analyzed using MIP in this current work are those from the bulk interpores spaces as observed and described with ESEM.

4. Discussion

The action of RHA in laterites based geopolymer composites yields better reactivity and more polycondensation together with the formation of more dense interpores spaces that in this case substitute the matrix. The laterites based geopolymer composites with high volume of RHA evidenced a fundamental difference for the standard curing at room temperature and the

curing at temperatures around 90 °C. While the curing at room temperature gave the flexural strength that remained between 8 and 12 MPa, as generally obtained with sand or fine aggregates added metakaolin based geopolymer composites (Kamseu et al. 2013; Kamseu et al. 2014), the curing around 90 °C resulted in a more complex microstructure in which geopolymer gel and iron silicates cover completely the fine aggregates with homogeneous distributed micropores (5-53µm). The combined action of geopolymer gel (polysialates and ferrosialates) and the iron silicates produced a particular dense interpores space that justifies the high flexural strength obtained: 30-40 MPa. The cumulative pore volume of the composites with the highest flexural strength was 93 and 120 mm^3/g (respectively for GPEL40 and GPOD40) relatively low with respect to the values of cumulative pore volume of silica-rich geopolymer composites (Kamseu et al. 2013; Kamseu et al. 2014; Kamseu et al. 2016) This could be considered just as the fraction of nanometric and fines micrometric pores since the final products of laterites based geopolymer composites present a porous nature. Appropriate investigations including the optimal microscope might permit to evaluate and quantify those of porosity that cannot, in this case, being investigate with the Mercury Intrusion porosimetry (MIP) (Kamseu et al. 2014). However there was no evident correlation between the pore volume and the mechanical strength due to the formation of good compact interpores spaces as from the polysialates, ferrosialates and iron silicates interconnection and densification.

It is important to note that the presence of amorphous/reactive silica from RHA firstly re-equilibrates the Si/Al and Si/Fe ratios in the laterites based geopolymer composites. In the context of optimum activation all these elements are dissolved into the alkaline solution and participate actively to the formation of polysialates/ferrosialates and iron silicates. The curing in a controlled humidity gave optimum reactive conditions for the better densification and strengthening mechanism. The presence of iron mineral was confirmed by FTIR spectra and XRD analysis, which revealed the insertion of iron atom within 3D network amorphous phase. The characteristics of end products obtained in this study help to validate our approach with objective to produce a high strength geopolymers from the N-A(Fe)-Si-H system in comparison to that of N-A-S-H. Further investigations with Mossbauer spectroscopy would help to give more details into the understanding of phases formation and the iron tranformations and reactivity.

5. Conclusions

Two laterites with similar degree of laterisation and iron content (~ 35 wt%) used in the present study as solid precursors were mixed with quartz sand, rice husk ash and alkaline solution for the production geopolymer composites under different curing conditions. The laterites based geopolymer composites appear more sustainable, low cost and environmentally-friendly. The solid precursors that do not need pretreatment appear ideal raw materials for the cleaner production of eco-friendly cements and composites.

The following conclusions can be derived:

- The addition of RHA resulted in a re-equilibrium of Si/Al and Si/Fe in the bulk compositions resulting in a significant improvement of the microstructure and mechanical properties;
- The laterites based geopolymer composites contain both polysialates and ferrosialates when curing at room temperature;
- In the context of controlled humidity and temperature around 90 °C, iron silicates complete polysialates and ferrosialates with the appearance of interconnected micro pores;
- The H_2O, the temperature and alkaline solution seem to play a significant role in the corrosion of metallic iron and development of micropores with particular dense inter pores spaces
- The band of nanometric pores generally present in geopolymer composites in the range of 0.01-0.1 μm shifted to lower values with peak at 0.00452 μm;
- The combined action of polysialates, ferrosialates and iron silicates forming a particular microstructure results in a very good mechanical properties (flexural strength ~ 30-40 MPa).

Further investigations will be carried out to strictly control the solid to water ratio in the geopolymeric pastes either during room temperature curing or in 60-100 °C range.

6. Acknowledgments

The authors are grateful to Ingessil S.r.l., Verona, Italy, for providing sodium silicate used in this study. This project received the contribution of the Academic of Science for the Third World TWAS through the funding grant no. 15-079 RG/CHE/AF/AC_I to Dr. Elie Kamseu.

7. References

Carlson, L., and U. Schwertmann. 1981. "Natural Ferrihydrites in Surface Deposits from Finland and Their Association with Silica." *Geochimica et Cosmochimica Acta* 45 (3). doi:10.1016/0016-7037(81)90250-7.

Cristiane, Gomes Kelly, G S T Lima, Torres Sandro Marden, D E Barros Silvio, Vasconcelos Igor Frota, and Barbosa Normando Perazzo. 2010. "Iron Distribution in Geopolymer with Ferromagnetic Rich Precursor" 643: 131–38. doi:10.4028/www.scientific.net/MSF.643.131.

Davidovits, J. 1988. "Geopolymers of the First Generation: SILIFACE-Process." In *Geopolymer '88 (volume1)*, 49–67.

Davidovits. F., J. Davidovits., M. Davidovits., R. Davidovits. 2012. Geopolymer cement of the calcium ferro-aluminosilicate polymer type and production process. WO/2012/056125, issued 2012.

Elimbi, A., H. K. Tchakoute, M. Kondoh, and J. Dika Manga. 2014. "Thermal Behavior and Characteristics of Fired Geopolymers Produced from Local Cameroonian Metakaolin." *Ceramics International* 40 (3): 4515–4520. doi:10.1016/j.ceramint.2013.08.126.

Farrell, D., .M. 1972. "A Study of the Infrared Absorption in the Oxidation of Magnetite to Maghemite and hematite:Mines Branch." *Inv. Rept 72-18*, 44.

Gallup, D. L. 1989. "Iron Silicate Scale Formation and Inhibition at the Salton Sea Geothermal Field." *Geothermics* 18 (1–2): 97–103. doi:10.1016/0375-6505(89)90015-1.

Gallup, D. L., and W. M. Reiff. 1991. "Characterization of Geothermal Scale Deposits by Fe-57 Mossbauer Spectroscopy and Complementary X-Ray Diffraction and Infrared Studies, Geothermics." *Geothermics* 20 (4): 207–24. doi:10.1016/0375-6505(91)90033-R.

Goodman, BA, JD Russell, and AR Fraser. 1976. "A MÖssbauer and IR Spectroscopic Study of the Structure of Nontronite." *Clays and Clay Minerals* 24: 53–59.

Heah, C. Y., H. Kamarudin, a. M. Mustafa Al Bakri, M. Bnhussain, M. Luqman, I. Khairul

Nizar, C. M. Ruzaidi, and Y. M. Liew. 2012. "Study on Solids-to-Liquid and Alkaline Activator Ratios on Kaolin-Based Geopolymers." *Construction and Building Materials* 35. Elsevier Ltd: 912–22. doi:10.1016/j.conbuildmat.2012.04.102.

Hofmeister, Anne M. 1987. "Single-Crystal Absorption and Reflection Infrared Spectroscopy of Forsterite and Fayalite." *Physics and Chemistry of Minerals* 14 (6): 499–513. doi:10.1007/BF00308285.

Jayasinghe, C., and R. S. Mallawaarachchi. 2009. "Flexural Strength of Compressed Stabilized Earth Masonry Materials." *Materials and Design* 30 (9): 3859–3868. doi:10.1016/j.matdes.2009.01.029.

K.C Gomes, S.M Torres, S. de Barros, N.P. Barbosa. 2007. "Geopolymer Bonded Steel Plates." In *ETDCM8- 8 Th Seminar on Experimental Techniques and Design in Composite Materials*.

Kamseu, E., L. M. Beleuk à Moungam, M. Cannio, Ndigui Billong, Duangrudee Chaysuwan, U. Chinje Melo, and C. Leonelli. 2017. "Substitution of Sodium Silicate with Rice Husk Ash-NaOH Solution in Metakaolin Based Geopolymer Cement Concerning Reduction in Global Warming." *Journal of Cleaner Production* 142: 3050–3060. doi:10.1016/j.jclepro.2016.10.164.

Kamseu, Elie, Maria Cannio, Esther A Obonyo, Fey Tobias, Maria Chiara, Vincenzo M Sglavo, and Cristina Leonelli. 2014. "Cement & Concrete Composites Metakaolin-Based Inorganic Polymer Composite : Effects of Fine Aggregate Composition and Structure on Porosity Evolution , Microstructure and Mechanical Properties." *CEMENT AND CONCRETE COMPOSITES* 53. Elsevier Ltd: 258–69. doi:10.1016/j.cemconcomp.2014.07.008.

Kamseu, Elie, Maria Chiara, U C Melo, Cristina Leonelli, and Vincenzo M Sglavo. 2013. "Design of Inorganic Polymer Cements : Effects of Matrix Strengthening on Microstructure." *Construction and Building Materials* 38. Elsevier Ltd: 1135–45. doi:10.1016/j.conbuildmat.2012.09.033.

Kamseu, Elie, Isabella Lancellotti, Vincenzo M. Sglavo, Luca Modolo, and Cristina Leonelli. 2016. "Design of Inorganic Polymer Mortar from Ferricalsialic and Calsialic Slags for Indoor Humidity Control." *Materials* 9 (6). doi:10.3390/ma9060410.

Kamseu, Elie, A. Nzeukou, P. Lemougna, Ndigui Billong, U.C. Melo, and C. Leonelli. 2013. "Induration of Laterites in the Tropical Areas. Assessment for Potential Structural

Applications." *Interceram* 62 (6): 430–37.

Kaze, R C, L M Beleuk, M L Fonkwe Djouka, A Nana, E Kamseu, U F Chinje Melo, and C Leonelli. 2017. "Applied Clay Science The Corrosion of Kaolinite by Iron Minerals and the Effects on Geopolymerization." *Applied Clay Science* 138. Elsevier B.V.: 48–62. doi:10.1016/j.clay.2016.12.040.

Keester, W. B. White and K. L. 1965. "The American Mineralogist, Vol. 50, September, 1965." *The American Mineralogist* 50 (1964).

Lassinantti, Magdalena, Marcello Romagnoli, Simone Pollastri, and Alessandro F Gualtieri. 2015. "Cement and Concrete Research Inorganic Polymers from Laterite Using Activation with Phosphoric Acid and Alkaline Sodium Silicate Solution : Mechanical and Microstructural Properties." *Cement and Concrete Research* 67. Elsevier Ltd: 259–70. doi:10.1016/j.cemconres.2014.08.010.

Moenke, H. H. W. 1974. "Silica, the Three-Dimensional Silicates, Borosilicates and Beryllium Silicates." In *The Infrared Spectra of Minerals*, edited by V. C. Farmer, Mineralogi, 365–82. Mineralogical Society of Great Britain and Ireland. doi:10.1180/mono-4.

N N Greenwood; T C Gibb. 1971. "Mössbauer Spectroscopy." *Kniha* 766: 669. doi:10.1007/978-1-61779-194-9_15.

Nik Ab Aziz, Nik Nurul Syuhada, Mazidah Mukri, Soenita Hashim, and Norazlan Khalid. 2015. "Influence of Compaction Effort for Laterite Soil Mix with Geopolymer in Designing Soil Liner." *Electronic Journal of Geotechnical Engineering* 20 (22): 12353–64.

Ninla, Patrick, Achille Balo, Elie Kamseu, Uphie Chinje, Marie-paule Delplancke, and Hubert Rahier. 2014. "Influence of the Processing Temperature on the Compressive Strength of Na Activated Lateritic Soil for Building Applications." *CONSTRUCTION & BUILDING MATERIALS* 65. Elsevier Ltd: 60–66. doi:10.1016/j.conbuildmat.2014.04.100.

Obonyo, Esther A., Elie Kamseu, Patrick N. Lemougna, Arlin B. Tchamba, Uphie C. Melo, and Cristina Leonelli. 2014. "A Sustainable Approach for the Geopolymerization of Natural Iron-Rich Aluminosilicate Materials." *Sustainability (Switzerland)* 6 (9): 5535–53. doi:10.3390/su6095535.

Polacci, Margherita, Don R Baker, and Liping Bai. 2008. "Large Vesicles Record Pathways of Degassing at Basaltic Volcanoes," 1023–29. doi:10.1007/s00445-007-0184-8.

Quong, R. 1976. *Scaling Characteristics in the Geothermal Loop Experimental Facility at Niland*. Edited by Lawrence Livermore National Laboratory. Report No.

Rees, Catherine A., John L. Provis, Grant C. Lukey, and Jannie S J Van Deventer. 2007. "Attenuated Total Reflectance Fourier Transform Infrared Analysis of Fly Ash Geopolymer Gel Aging." *Langmuir* 23 (15): 8170–79. doi:10.1021/la700713g.

Schwertmann, U., and H. Thalmann. 1976. "The Influence of [Fe(II)], [Si], and pH on the Formation of Lepidocrocite and Ferrihydrite during Oxidation of Aqueous FeCl2 Solutions." *Clay Miner.* 11: 189–99.

Sidhu, P. S. 1988. "Transformation of Trace Element-Substituted Maghemite to Hematite." *Clays and Clay Minerals* 36 (1): 31–38. doi:10.1346/CCMN.1988.0360105.

Sore, Seick Omar, Adamah Messan, Elodie Prud'homme, Gilles Escadeillas, and Fran??ois Tsobnang. 2016. "Synthesis and Characterization of Geopolymer Binders Based on Local Materials from Burkina Faso Metakaolin and Rice Husk Ash." *Construction and Building Materials* 124: 301–11. doi:10.1016/j.conbuildmat.2016.07.102.

Subaer. 2004. "Influence of Aggregate on the Microstructure of Geopolymer." Curtin University of Technology, Western Australia,.

Tchakouté, Hervé K., Claus H. Rüscher, Sakeo Kong, Elie Kamseu, and Cristina Leonelli. 2016. "Comparison of Metakaolin-Based Geopolymer Cements from Commercial Sodium Waterglass and Sodium Waterglass from Rice Husk Ash." *Journal of Sol-Gel Science and Technology* 78 (3). Springer US: 492–506. doi:10.1007/s10971-016-3983-6.

Vempati, R. K., R. K. Vempati, and R. H. Loeppert. 1989. "Influence of Structural and Adsorbed Si on the Transformation of Synthetic Ferrihydrite." *CLAYS CLAY MINER*, 273--279.

Figures and Tables captions

- High strength matrices is designed used natural iron-rich aluminosilicates
- Polymer matrices need less energy and lower global warming potential
- Polysialates, ferrosialates and ferrosilicates are combined into an optimal matrix

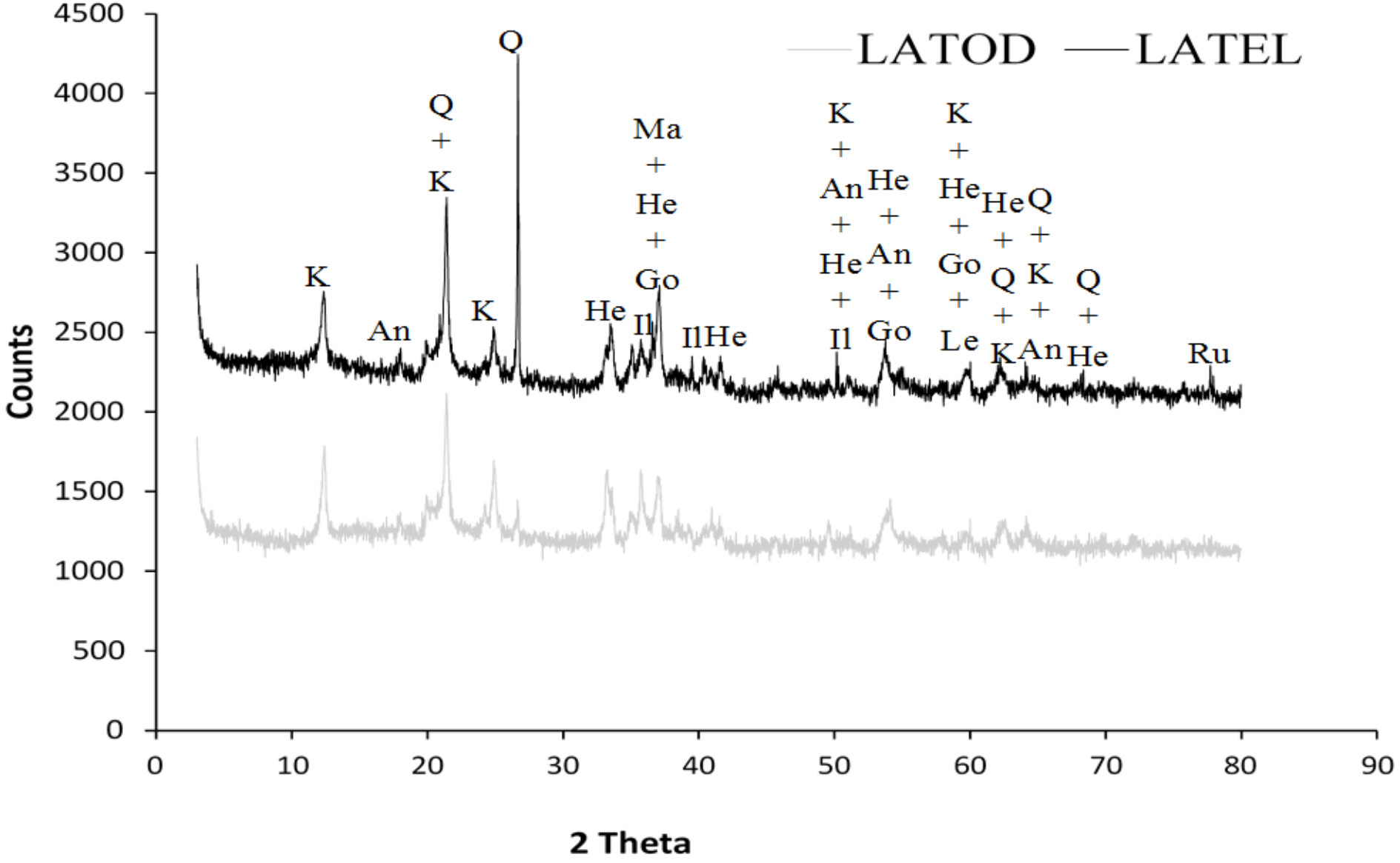
LATOD
LATEL
Counts
2 Theta
4500
4000
3500
3000
2500
2000
1500
1000
500
0
0
10
20
30
40
50
60
70
80
90
K
An
Q + K
K
Q
He
Ma + He + Go
Il
IlHe
K + An + He + Il
He + An + Go
K + He + Go + Le
He
Q + K + Q + K + An
Q + He
Ru

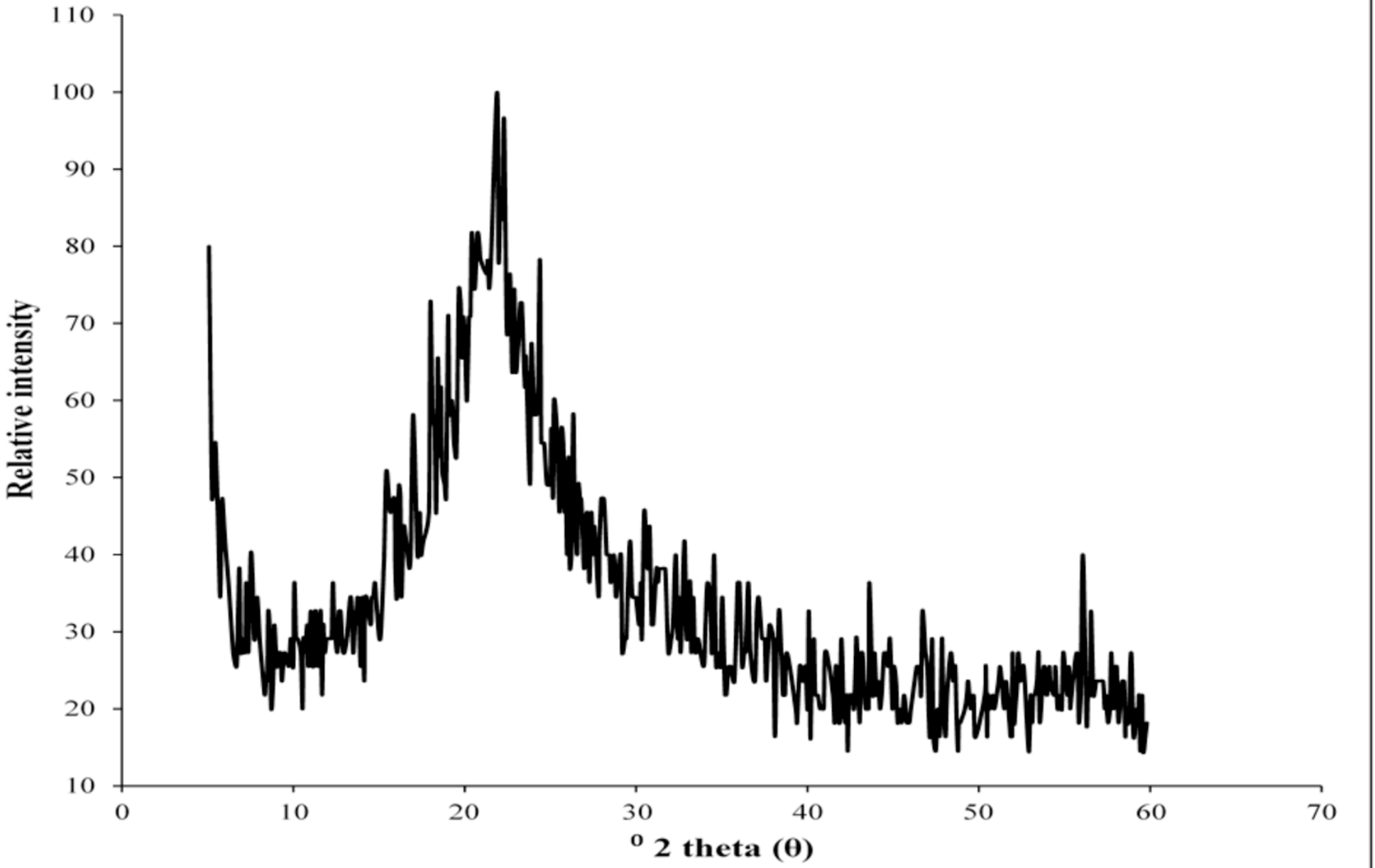
Relative intensity
110
100
90
80
70
60
50
40
30
20
10
0
10
20
30
40
50
60
70
o 2 theta (θ)

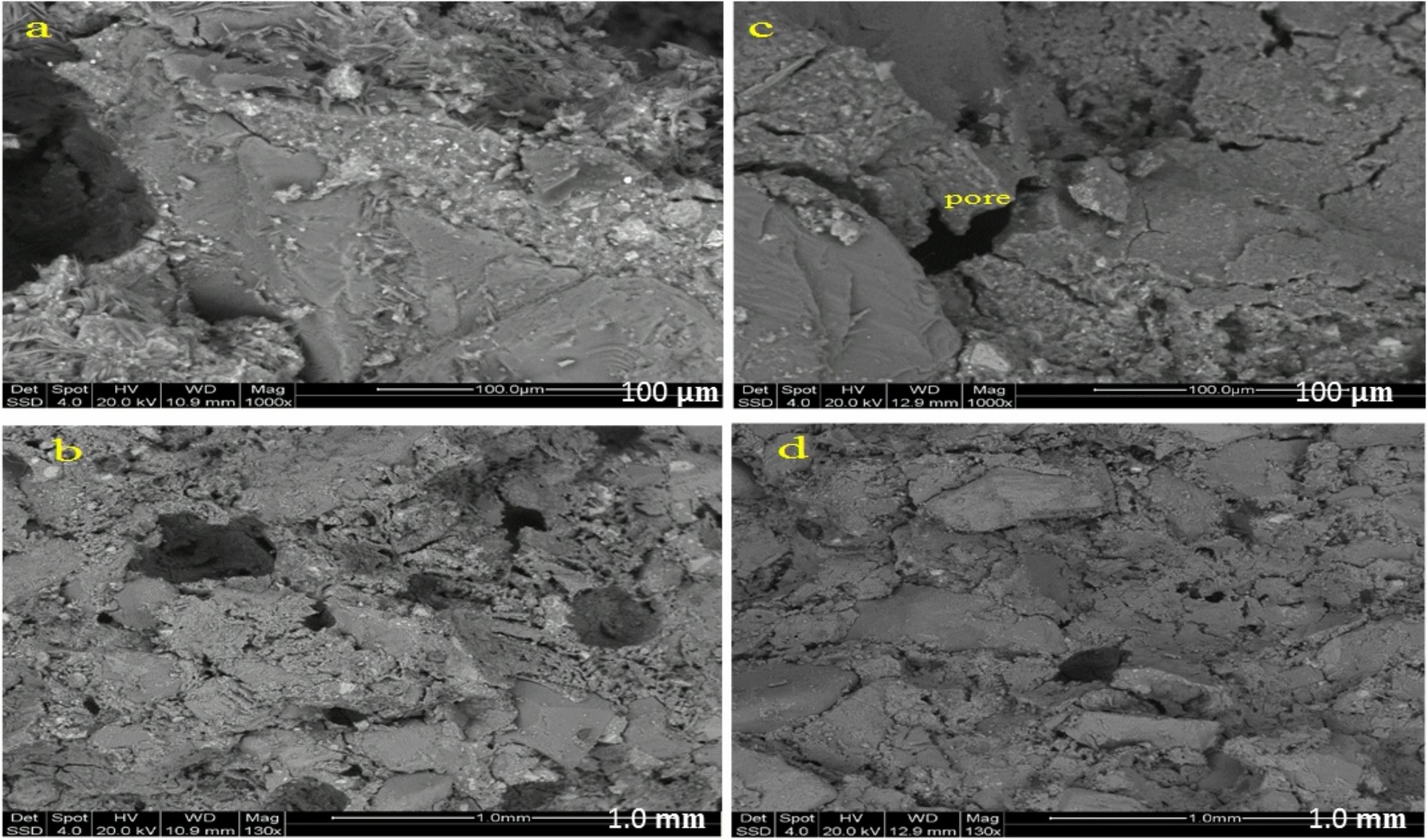
a
Det SSD
Spot 4.0
HV 20.0 kV
WD 10.9 mm
Mag 1000x
100.0µm
100 µm
c
pore
Det SSD
Spot 4.0
HV 20.0 kV
WD 12.9 mm
Mag 1000x
100.0µm
100 µm
b
Det SSD
Spot 4.0
HV 20.0 kV
WD 10.9 mm
Mag 130x
1.0mm
1.0 mm
d
Det SSD
Spot 4.0
HV 20.0 kV
WD 12.9 mm
Mag 130x
1.0mm
1.0 mm

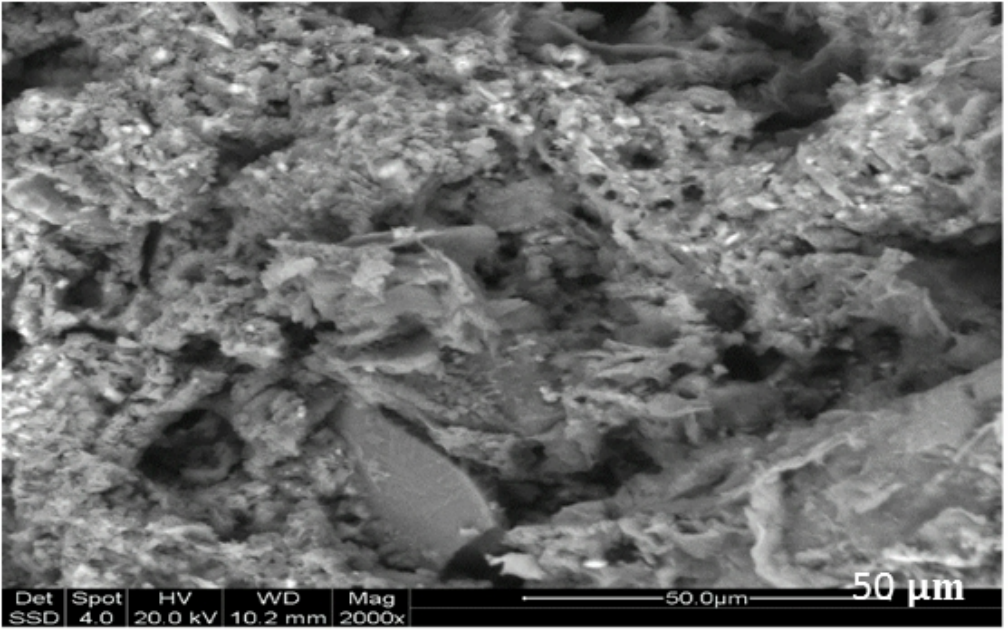
Det SSD
Spot 4.0
HV 20.0 kV
WD 10.2 mm
Mag 2000x
50.0µm
50 µm

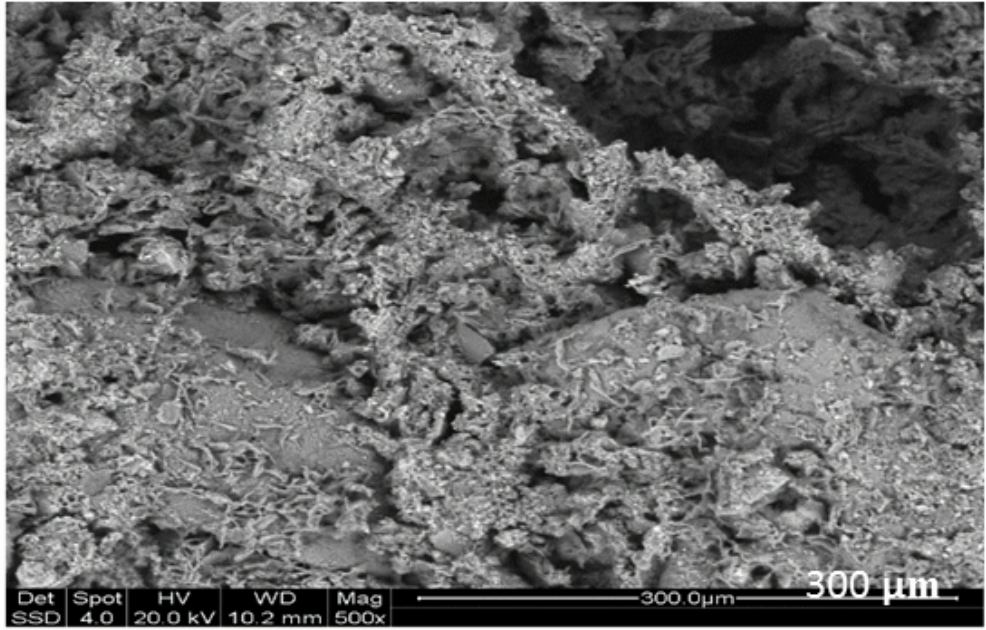
Det SSD
Spot 4.0
HV 20.0 kV
WD 10.2 mm
Mag 500x
300.0µm
300 µm

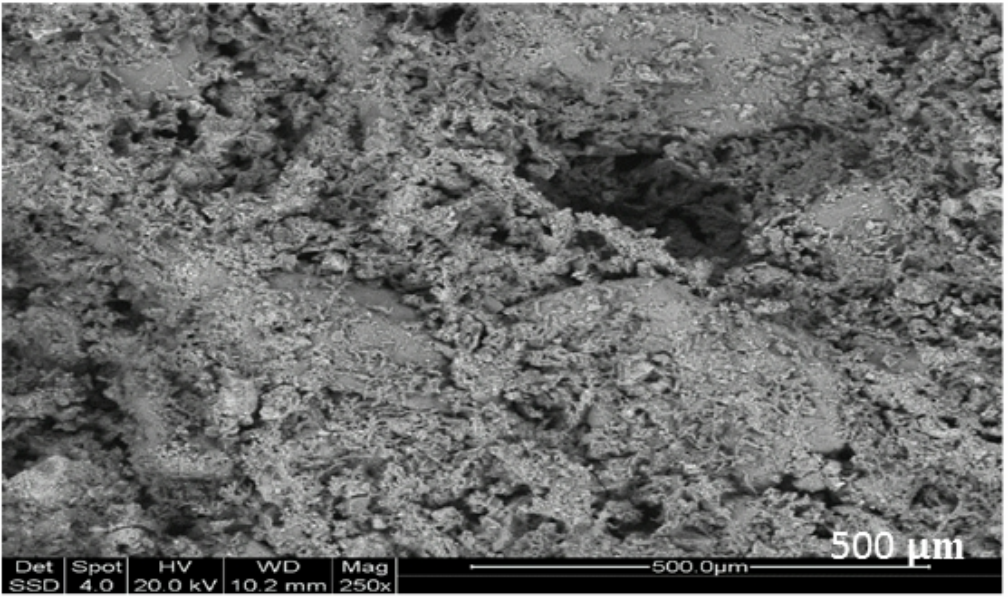
Det SSD
Spot 4.0
HV 20.0 kV
WD 10.2 mm
Mag 250x
500.0µm
500 µm

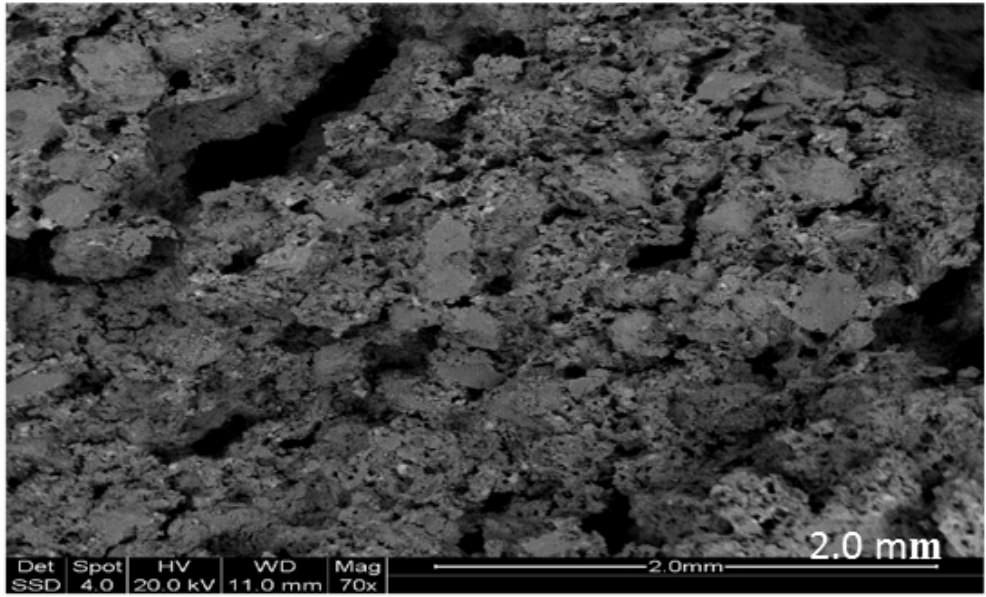
Det SSD
Spot 4.0
HV 20.0 kV
WD 11.0 mm
Mag 70x
2.0mm
2.0 mm

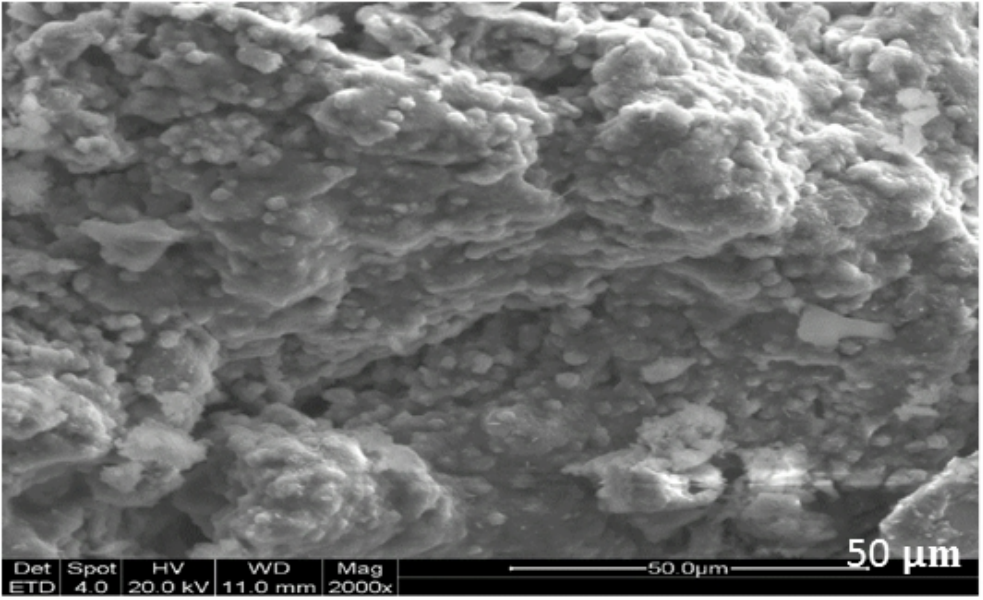
Det Spot HV WD Mag
ETD 4.0 20.0 kV 11.0 mm 2000x
50.0µm
50 µm

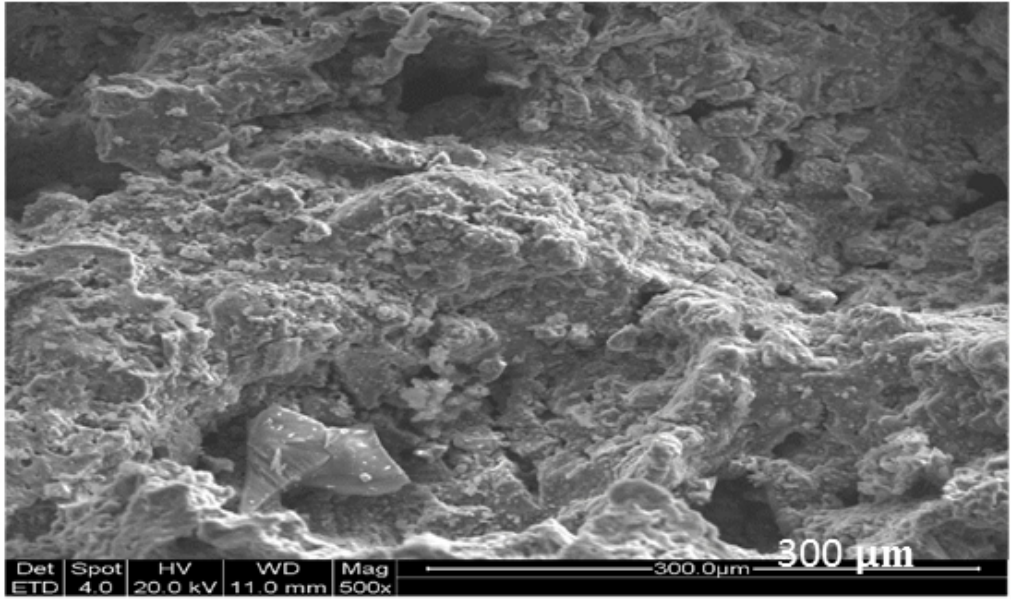
Det Spot HV WD Mag
ETD 4.0 20.0 kV 11.0 mm 500x
300.0µm
300 µm

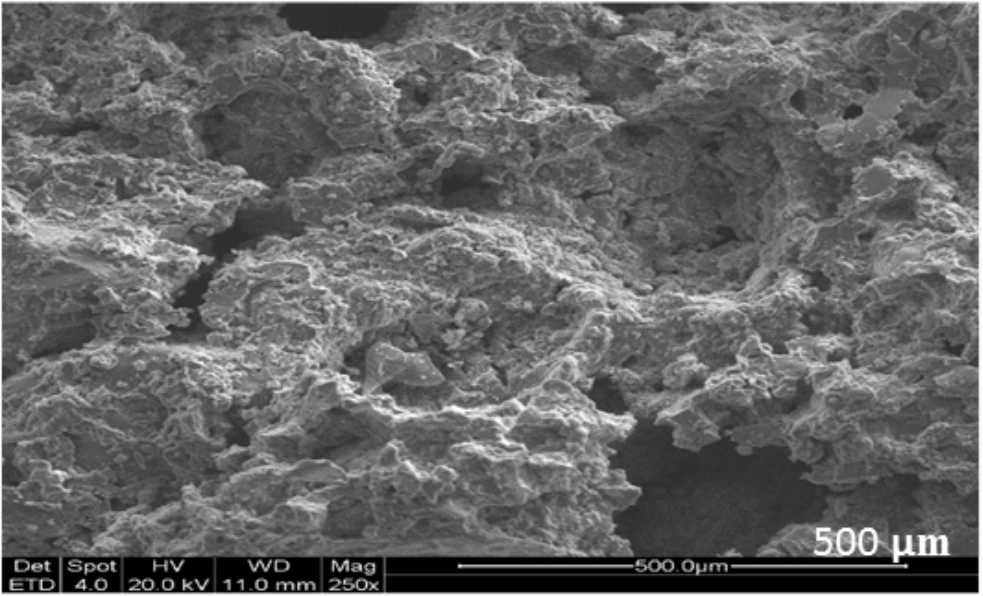
Det Spot HV WD Mag
ETD 4.0 20.0 kV 11.0 mm 250x
500.0µm
500 µm

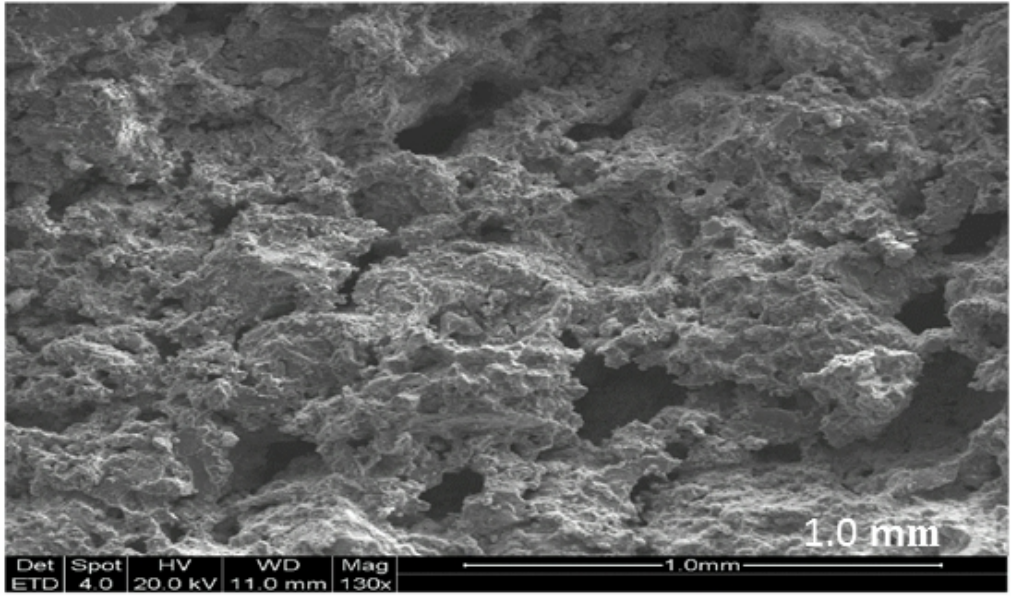
Det Spot HV WD Mag
ETD 4.0 20.0 kV 11.0 mm 130x
1.0mm
1.0 mm

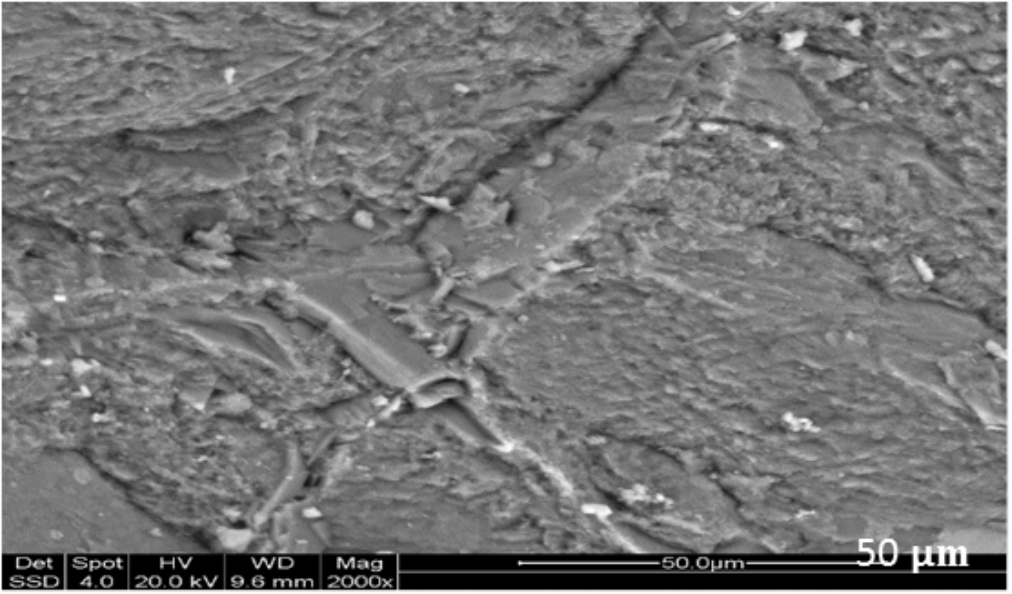
Det SSD
Spot 4.0
HV 20.0 kV
WD 9.6 mm
Mag 2000x
50.0µm
50 µm

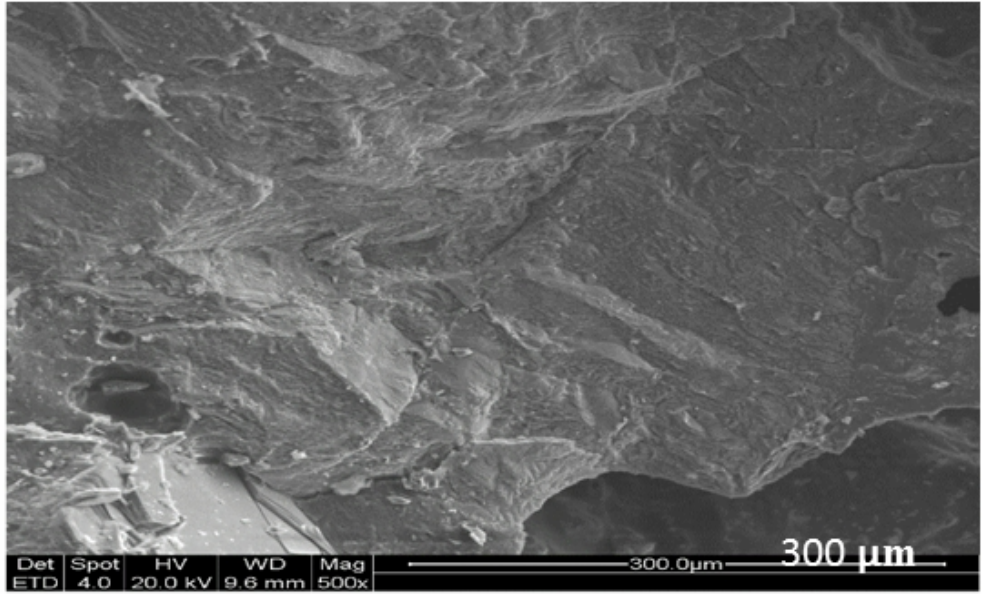
Det ETD
Spot 4.0
HV 20.0 kV
WD 9.6 mm
Mag 500x
300.0µm
300 µm

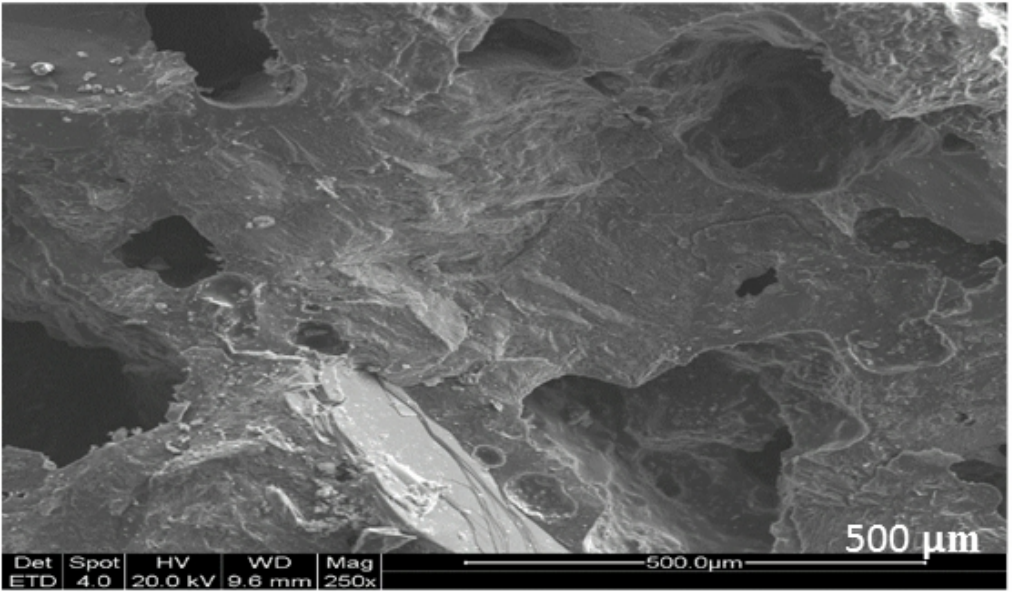
Det ETD
Spot 4.0
HV 20.0 kV
WD 9.6 mm
Mag 250x
500.0µm
500 µm

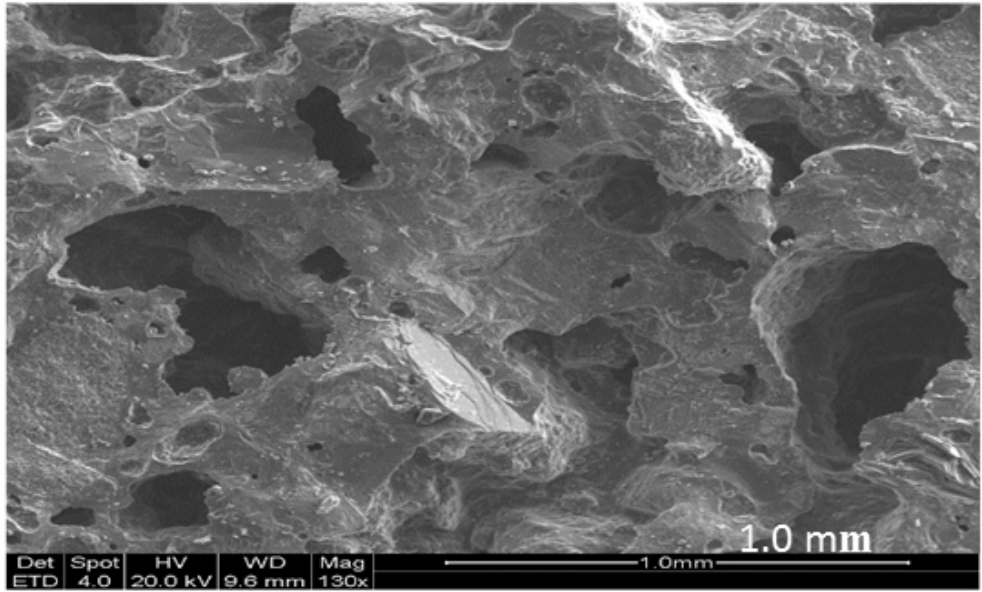
Det ETD
Spot 4.0
HV 20.0 kV
WD 9.6 mm
Mag 130x
1.0mm
1.0 mm

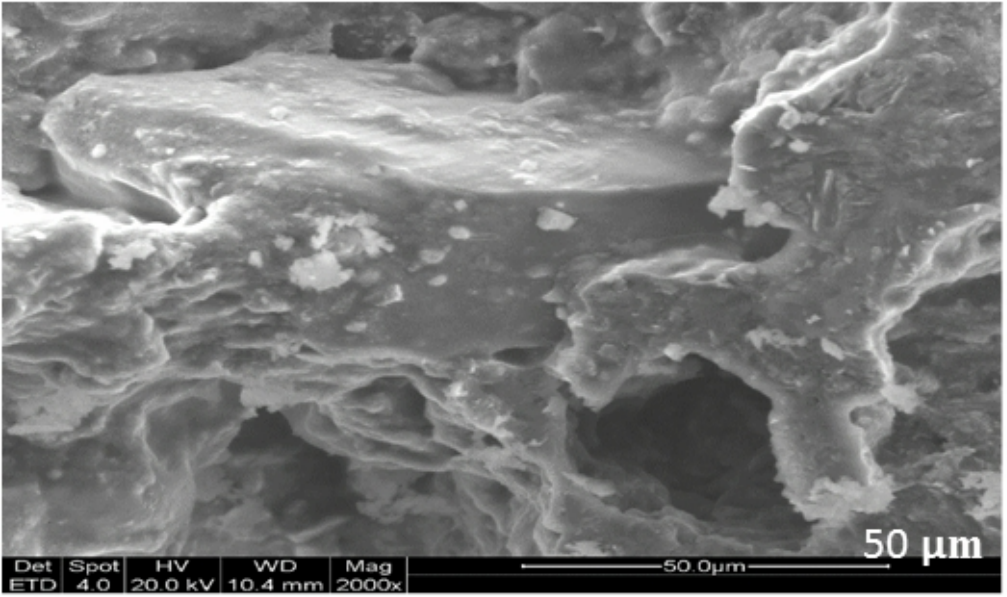
50 µm
Det Spot HV WD Mag
ETD 4.0 20.0 kV 10.4 mm 2000x
50.0µm

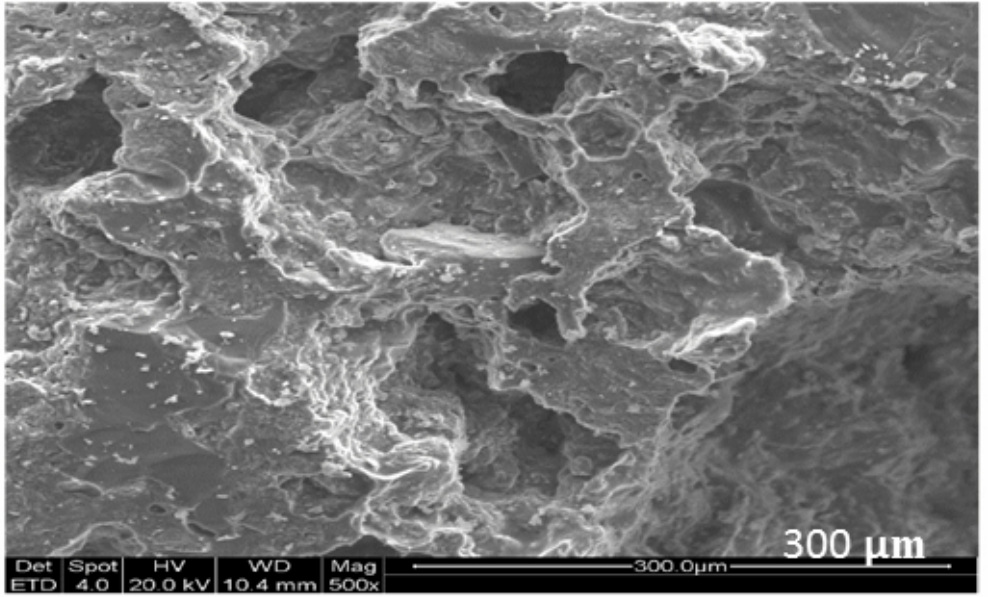
300 µm
Det Spot HV WD Mag
ETD 4.0 20.0 kV 10.4 mm 500x
300.0µm

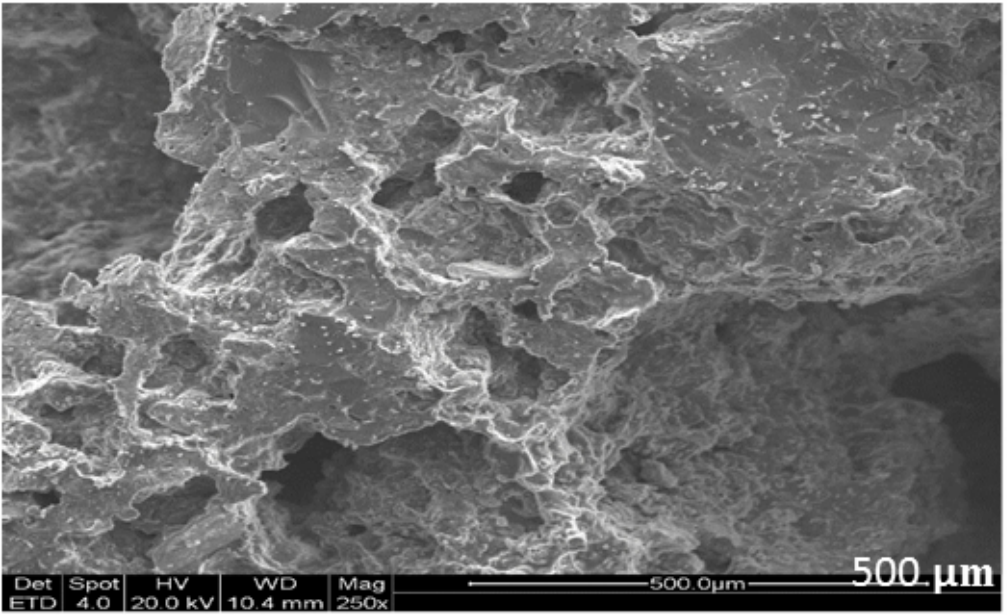
500 µm
Det Spot HV WD Mag
ETD 4.0 20.0 kV 10.4 mm 250x
500.0µm

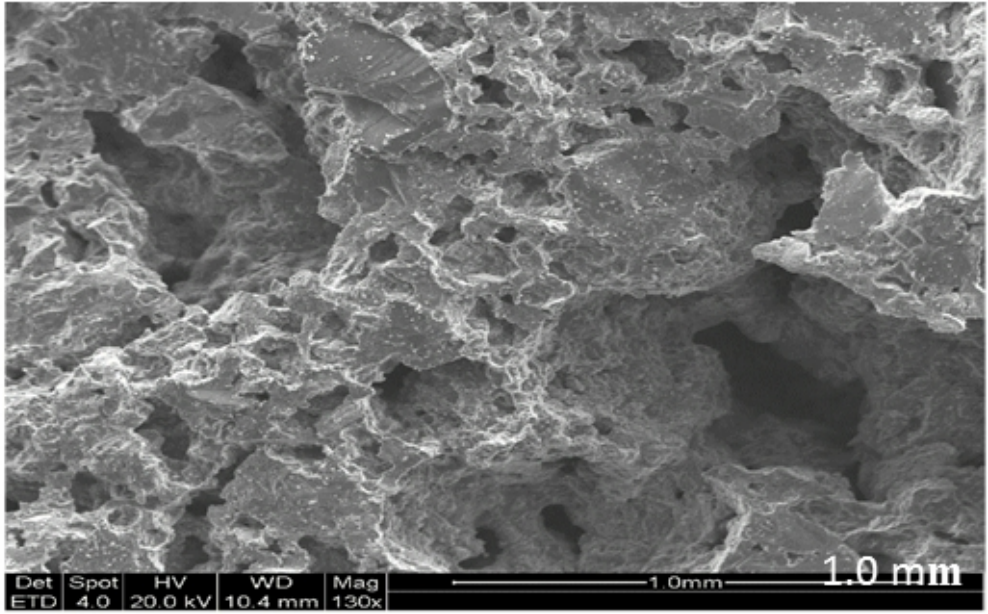
1.0 mm
Det Spot HV WD Mag
ETD 4.0 20.0 kV 10.4 mm 130x
1.0mm

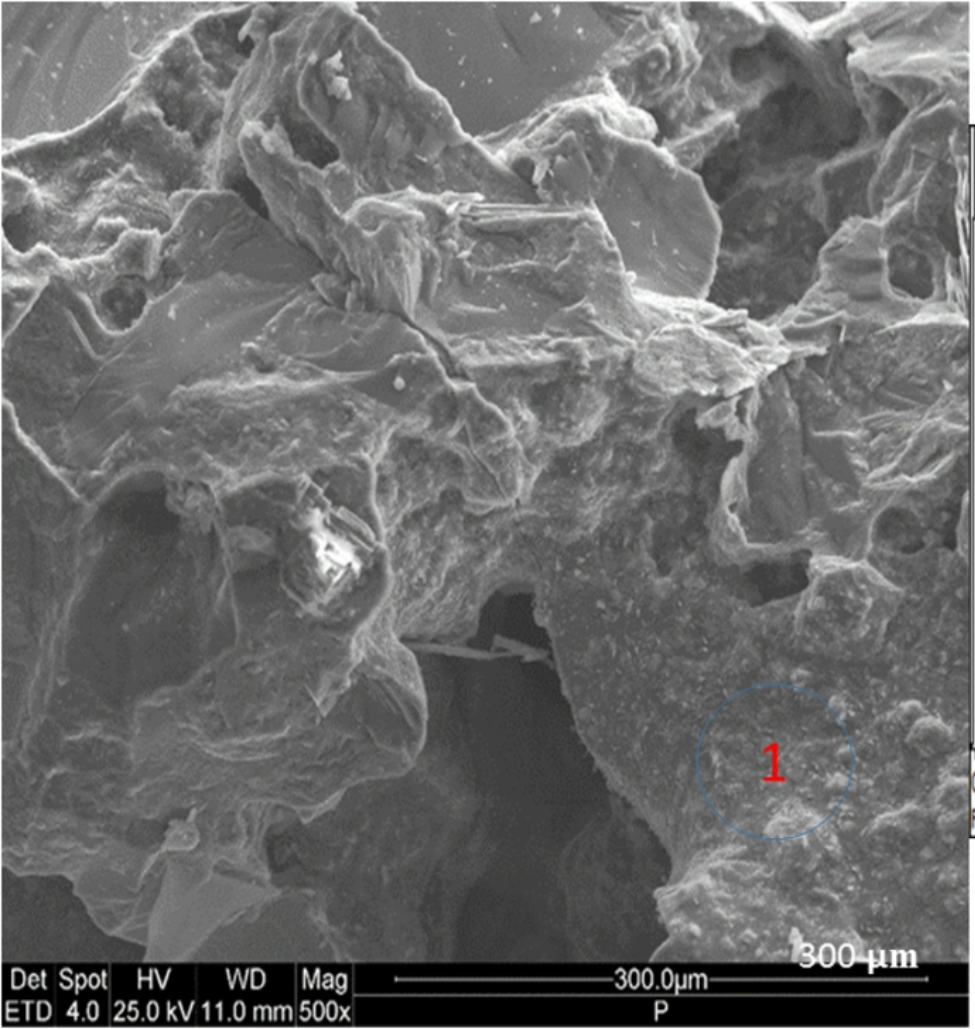
1
300 µm
Det Spot HV WD Mag
ETD 4.0 25.0 kV 11.0 mm 500x
300.0µm
P

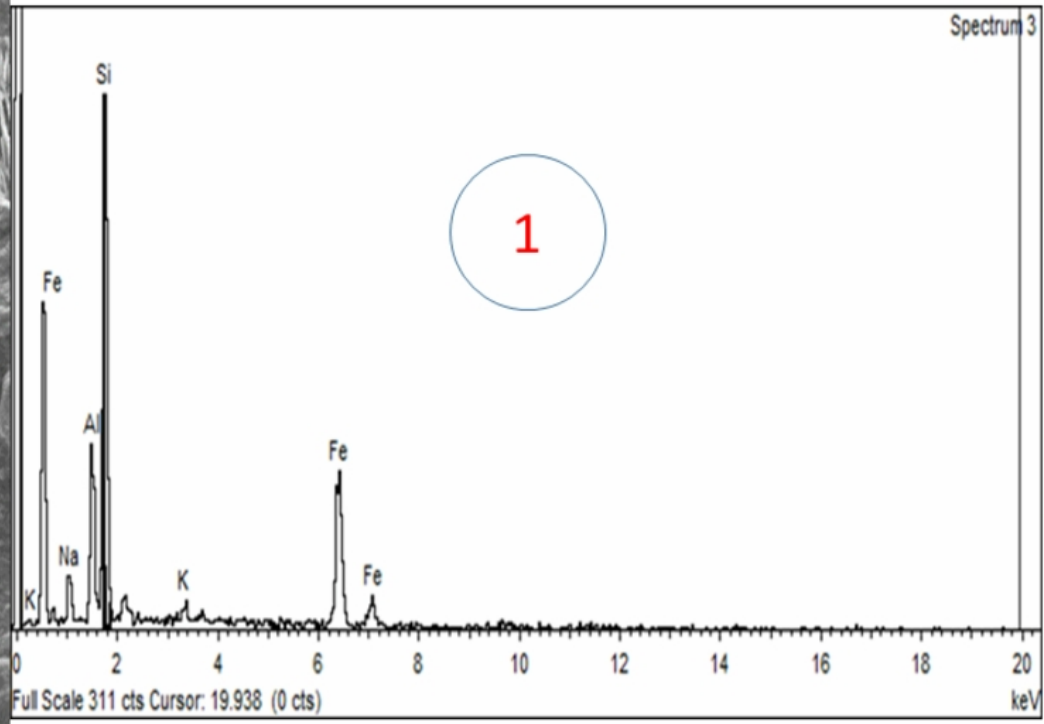
Spectrum 3
1
Si
Fe
Al
Na
K
K
Fe
Fe
0
2
4
6
8
10
12
14
16
18
20
Full Scale 311 cts Cursor: 19.938 (0 cts)
keV

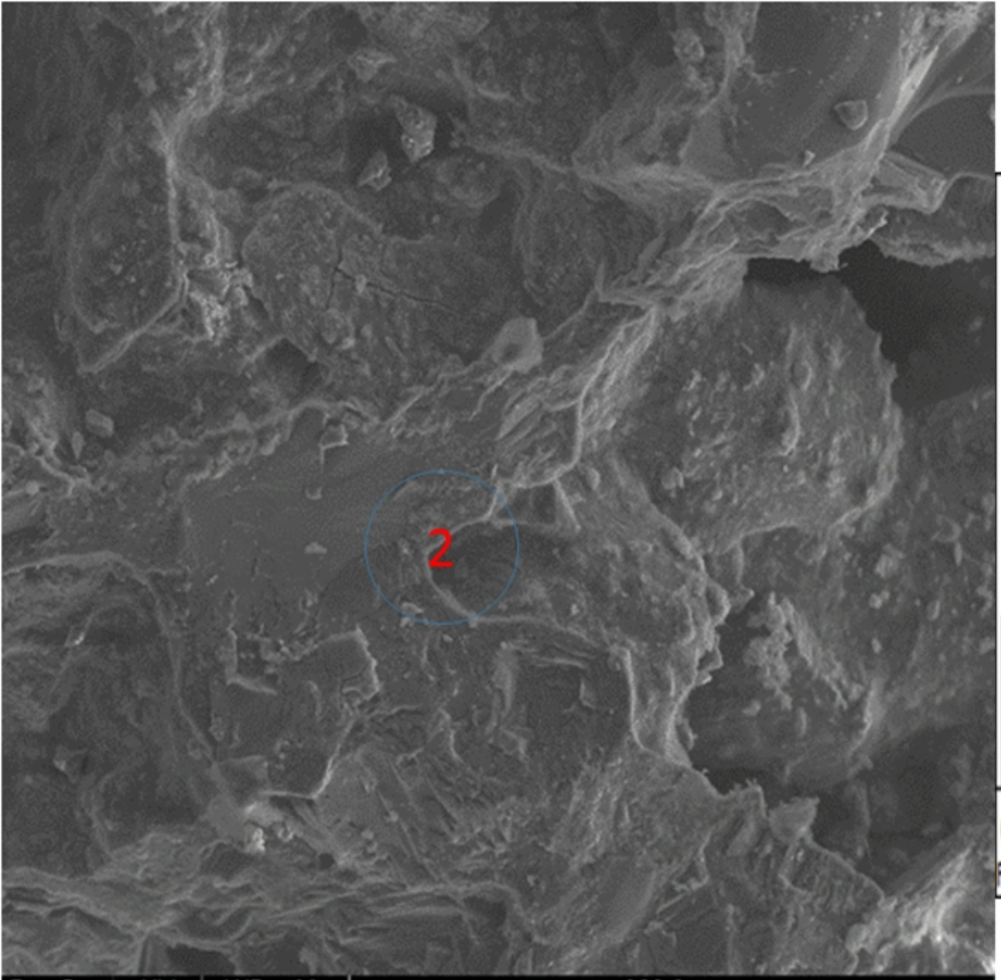
2
Det Spot HV WD Mag
ETD 4.0 20.0 kV 9.9 mm 500x
300.0µm
P

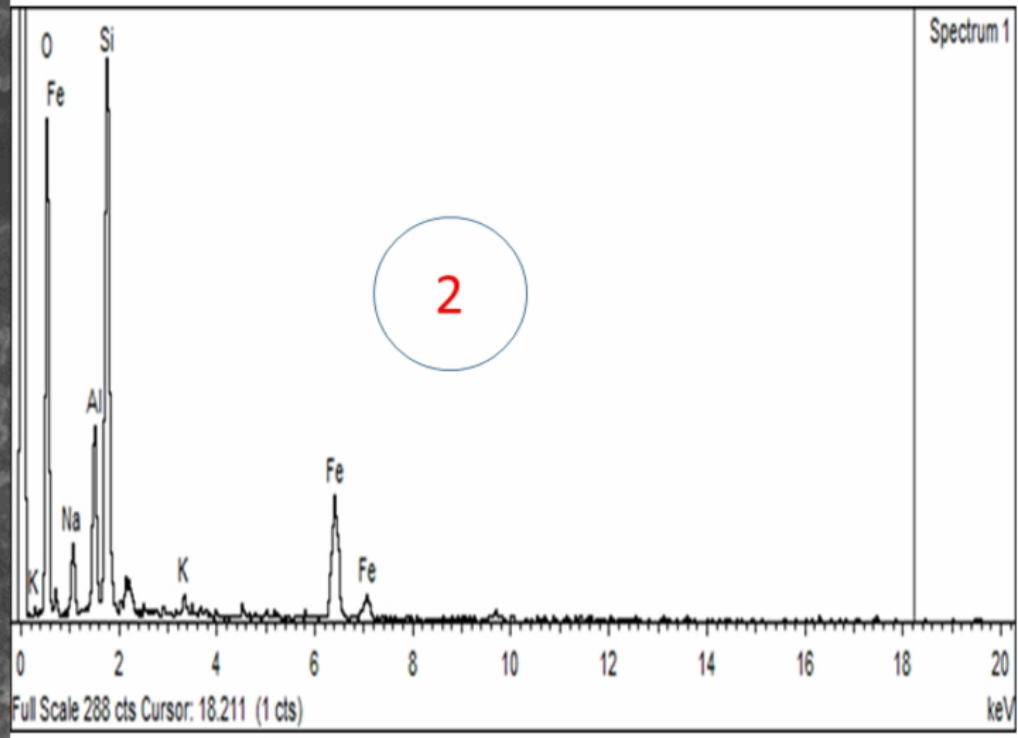
Spectrum 1
O
Fe
Si
Al
Na
K
K
Fe
Fe
2
0 2 4 6 8 10 12 14 16 18 20
Full Scale 288 cts Cursor: 18.211 (1 cts)
keV

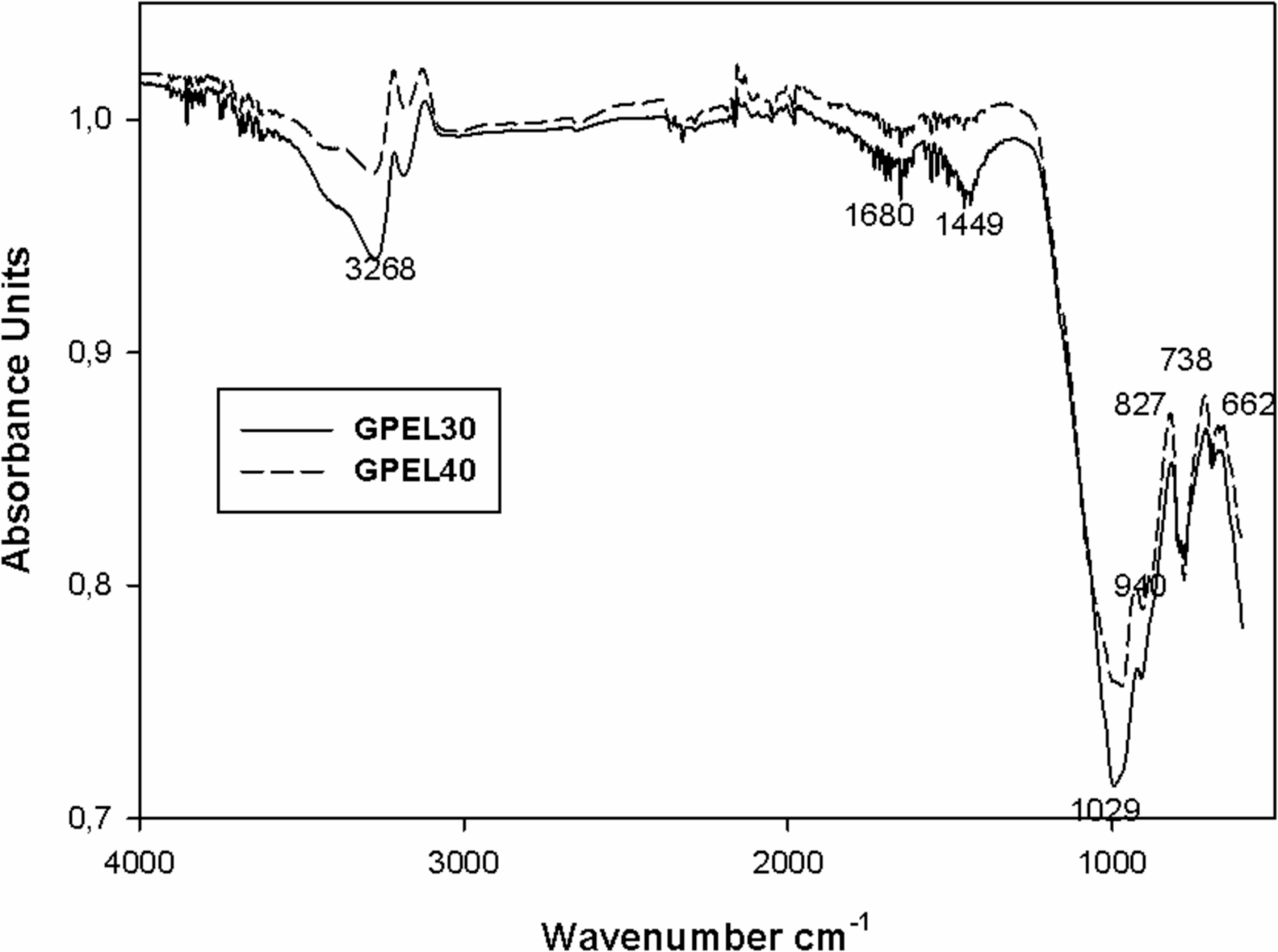
1,0
0,9
0,8
0,7
Absorbance Units
4000
3000
2000
1000
Wavenumber cm-1
GPEL30
GPEL40
3268
1680
1449
1029
940
827
738
662

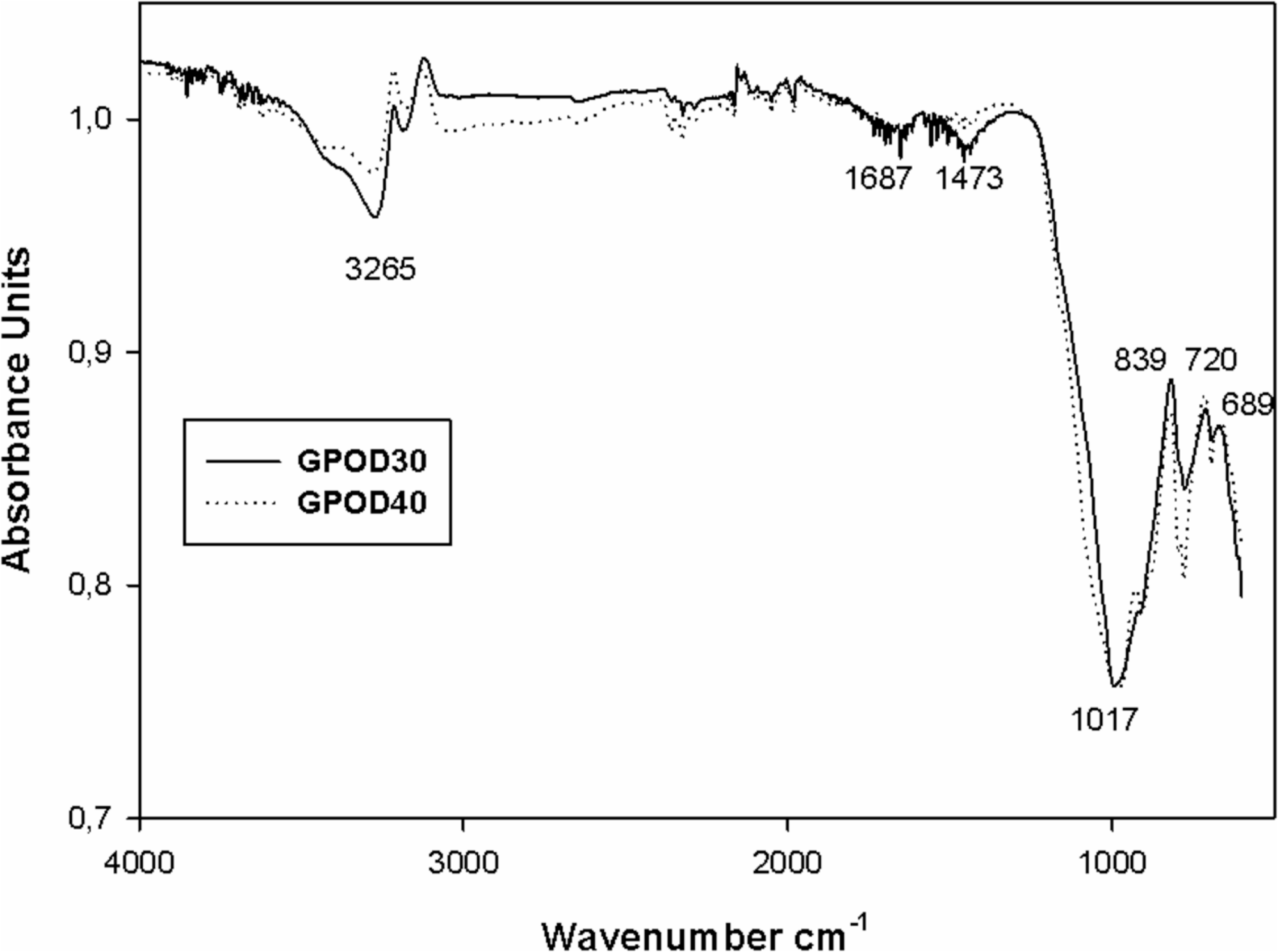
1,0
0,9
0,8
0,7
Absorbance Units
3265
1687
1473
839
720
689
1017
GPOD30
GPOD40
4000
3000
2000
1000
Wavenumber cm-1

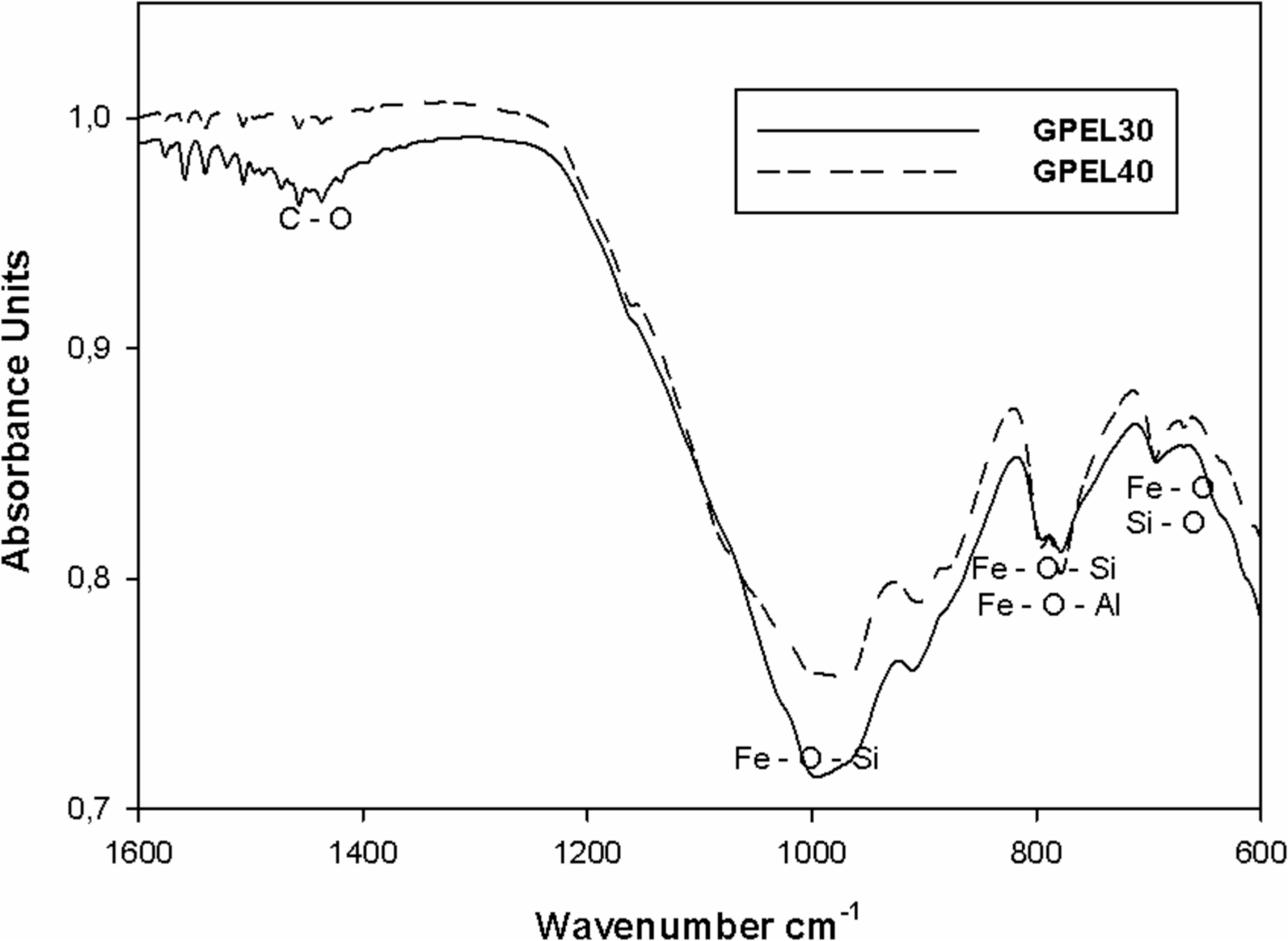
GPEL30
GPEL40
C - O
Fe - O - Si
Fe - O - Si
Fe - O - Al
Fe - O
Si - O
Absorbance Units
1,0
0,9
0,8
0,7
1600
1400
1200
1000
800
600
Wavenumber cm-1

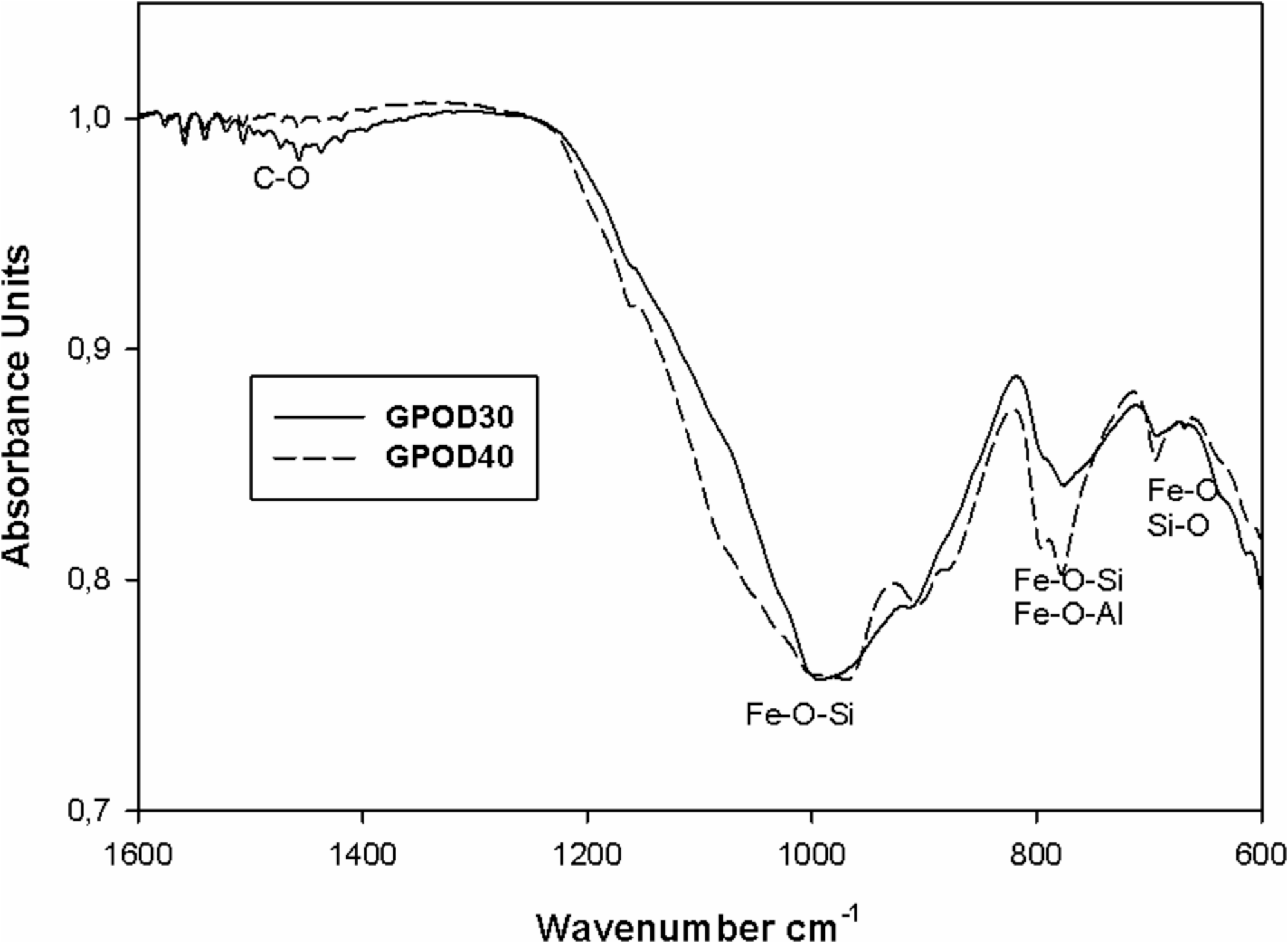
1,0
0,9
0,8
0,7
Absorbance Units
C-O
GPOD30
GPOD40
Fe-O-Si
Fe-O-Si
Fe-O-Al
Fe-O
Si-O
1600
1400
1200
1000
800
600
Wavenumber cm-1

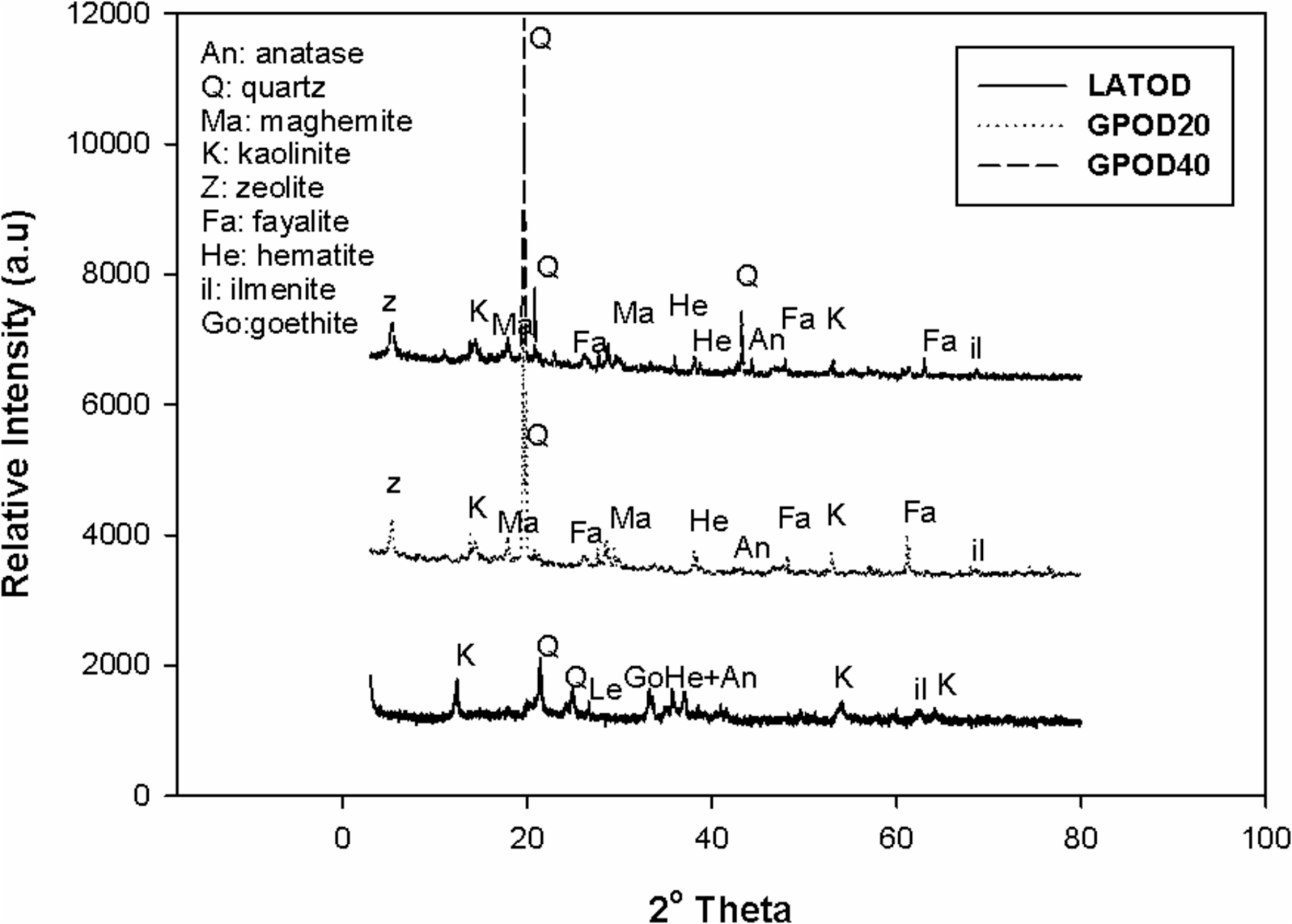
An: anatase
Q: quartz
Ma: maghemite
K: kaolinite
Z: zeolite
Fa: fayalite
He: hematite
il: ilmenite
Go:goethite
LATOD
GPOD20
GPOD40
Relative Intensity (a.u)
2° Theta
12000
10000
8000
6000
4000
2000
0
0
20
40
60
80
100
Q
z
K
Ma
Fa
Ma
He
Q
He
An
Fa
K
Fa
il
Q
z
K
Ma
Fa
Ma
He
An
Fa
K
Fa
il
K
Q
Q
Le
Go
He+An
K
il
K

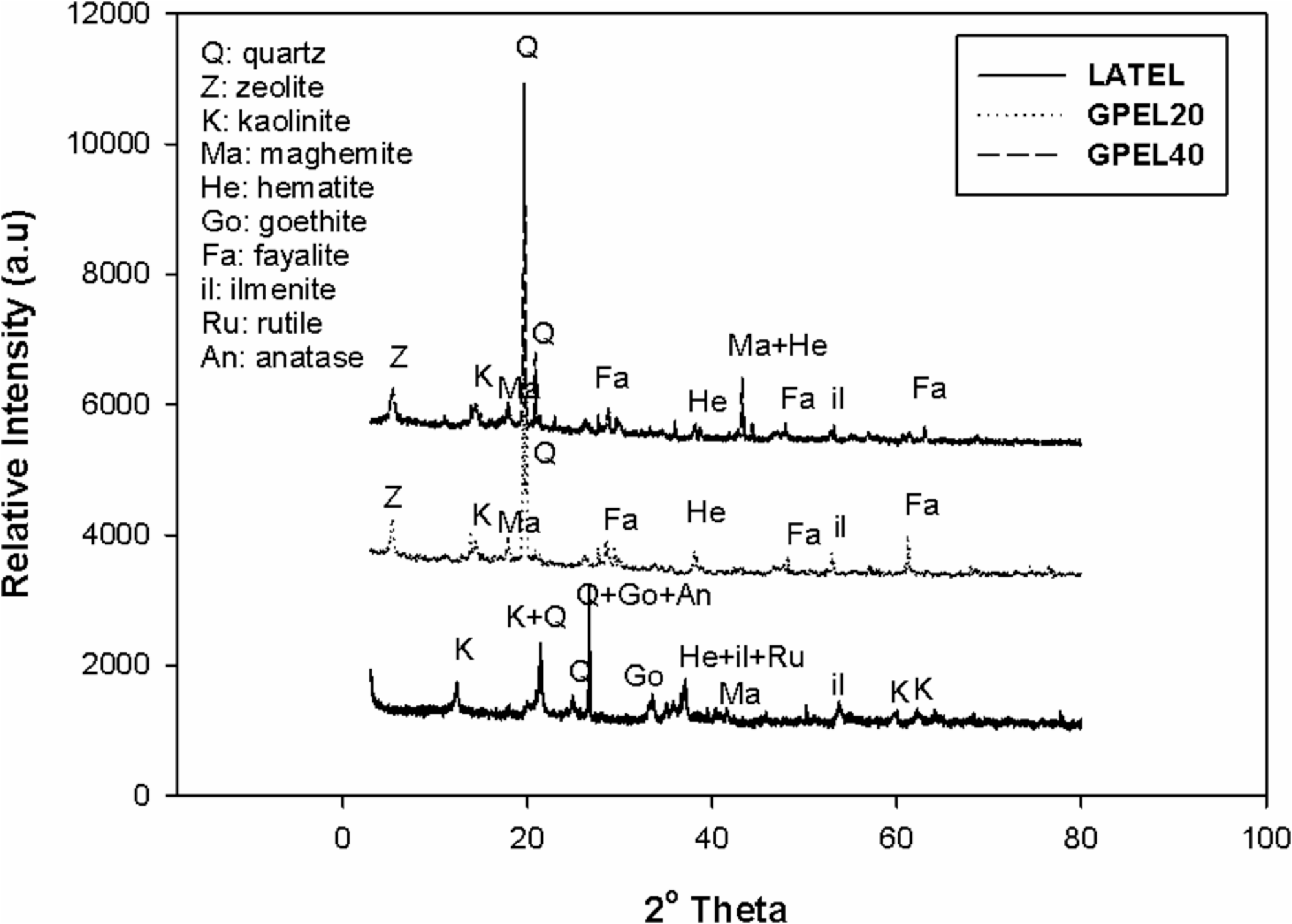
Q: quartz
Z: zeolite
K: kaolinite
Ma: maghemite
He: hematite
Go: goethite
Fa: fayalite
il: ilmenite
Ru: rutile
An: anatase
LATEL
GPEL20
GPEL40
Relative Intensity (a.u)
2° Theta
12000
10000
8000
6000
4000
2000
0
0
20
40
60
80
100
Q
Z
K
Ma
Fa
He
Ma+He
Fa
il
Fa
Q
Z
K
Ma
Fa
He
Fa
il
Fa
Q+Go+An
K+Q
K
Q
Go
He+il+Ru
Ma
il
K
K

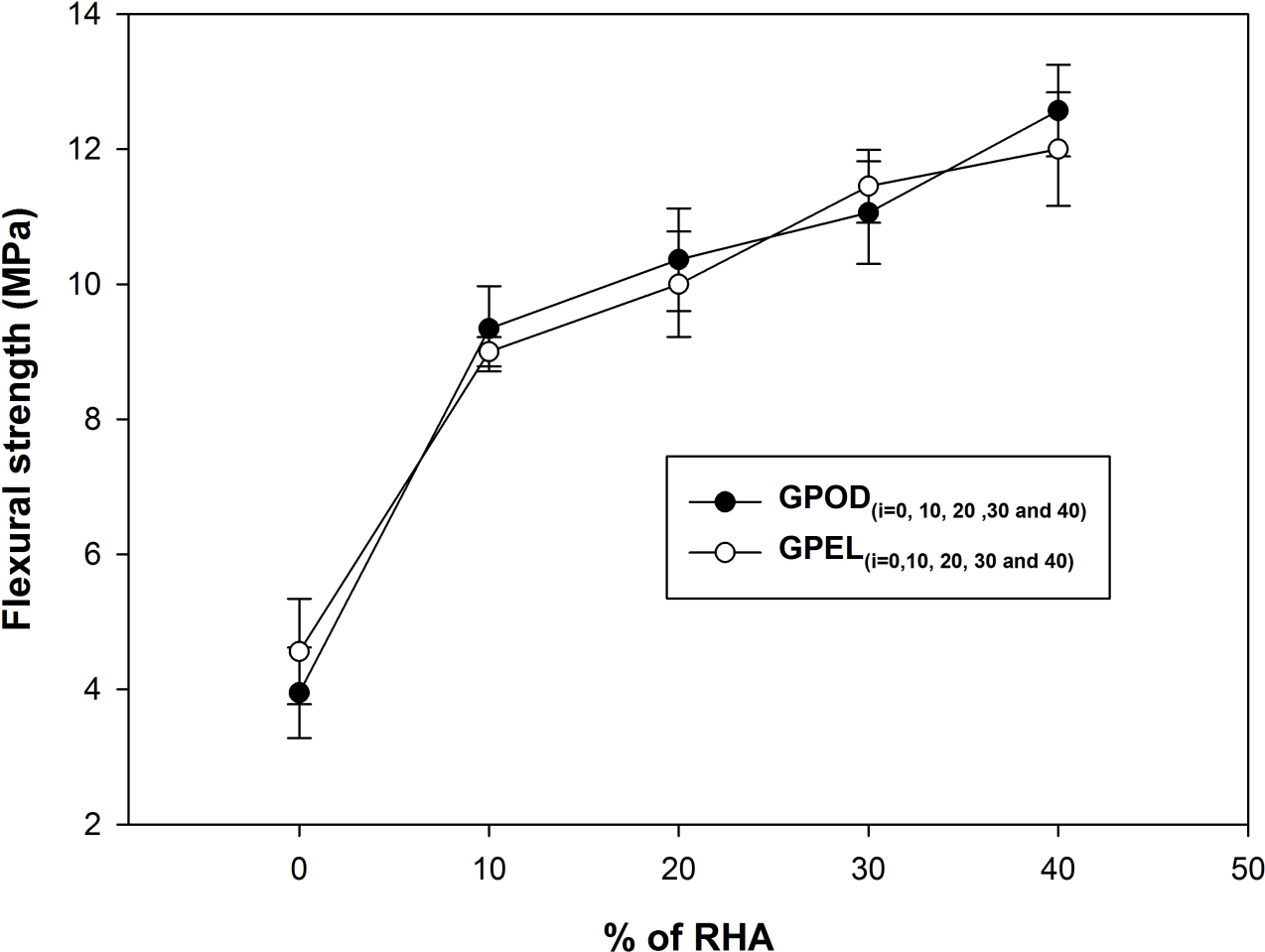
Flexural strength (MPa)
14
12
10
8
6
4
2
0
10
20
30
40
50
% of RHA
GPOD(i=0, 10, 20 ,30 and 40)
GPEL(i=0,10, 20, 30 and 40)

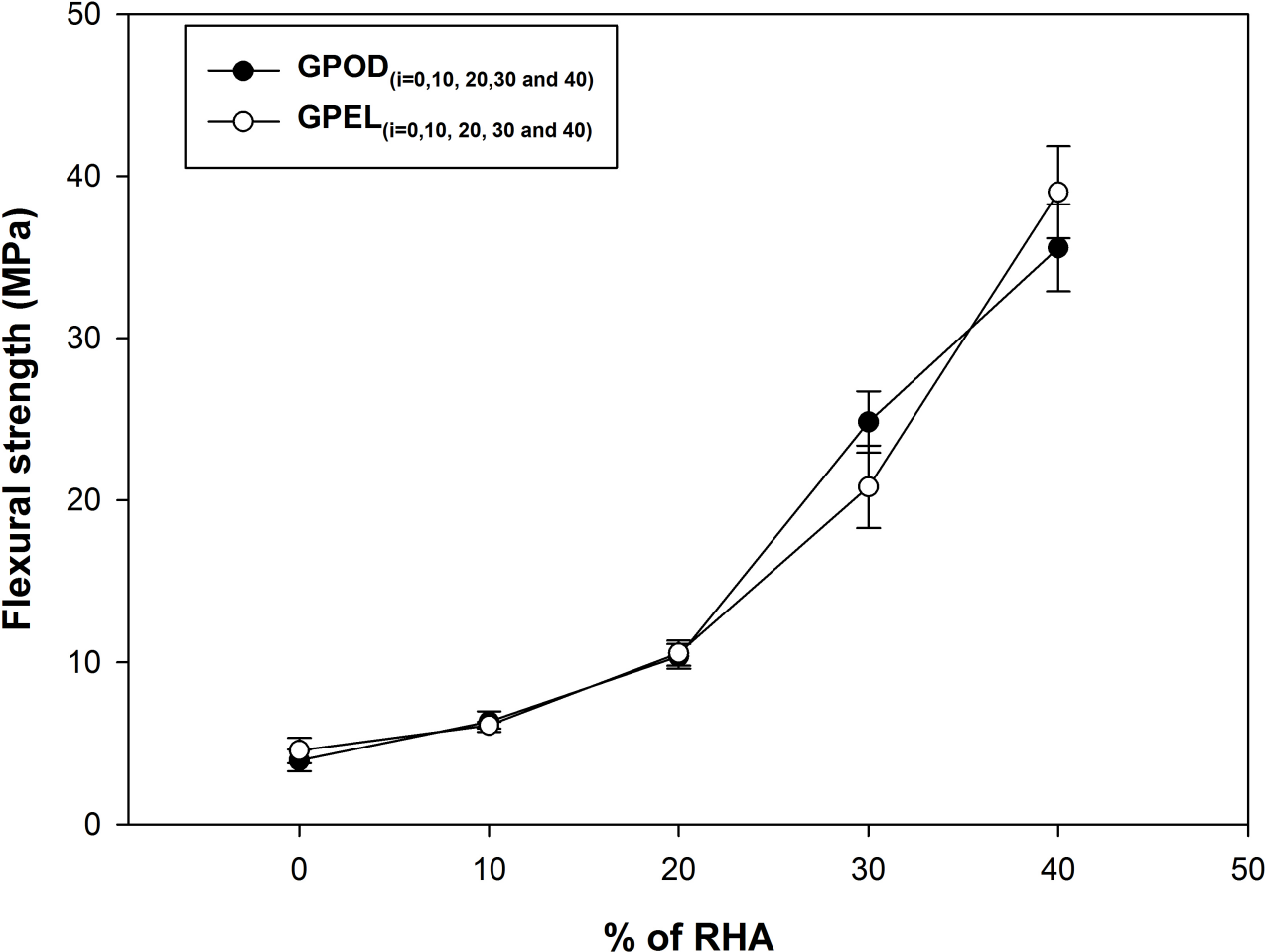
GPOD(i=0,10, 20,30 and 40)
GPEL(i=0,10, 20, 30 and 40)
Flexural strength (MPa)
0
10
20
30
40
50
0
10
20
30
40
50
% of RHA

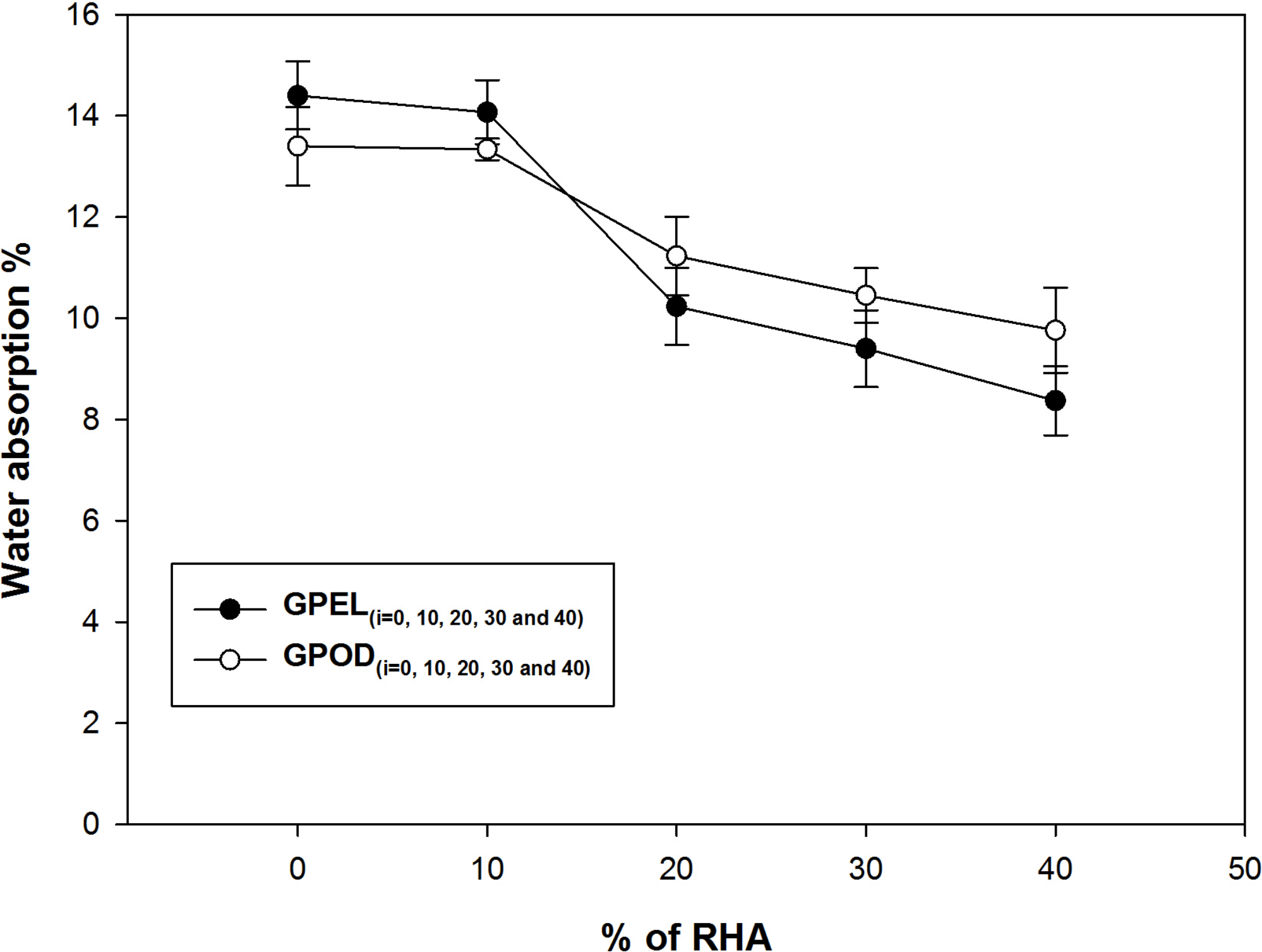
Water absorption %
% of RHA
0
2
4
6
8
10
12
14
16
0
10
20
30
40
50
GPEL(i=0, 10, 20, 30 and 40)
GPOD(i=0, 10, 20, 30 and 40)

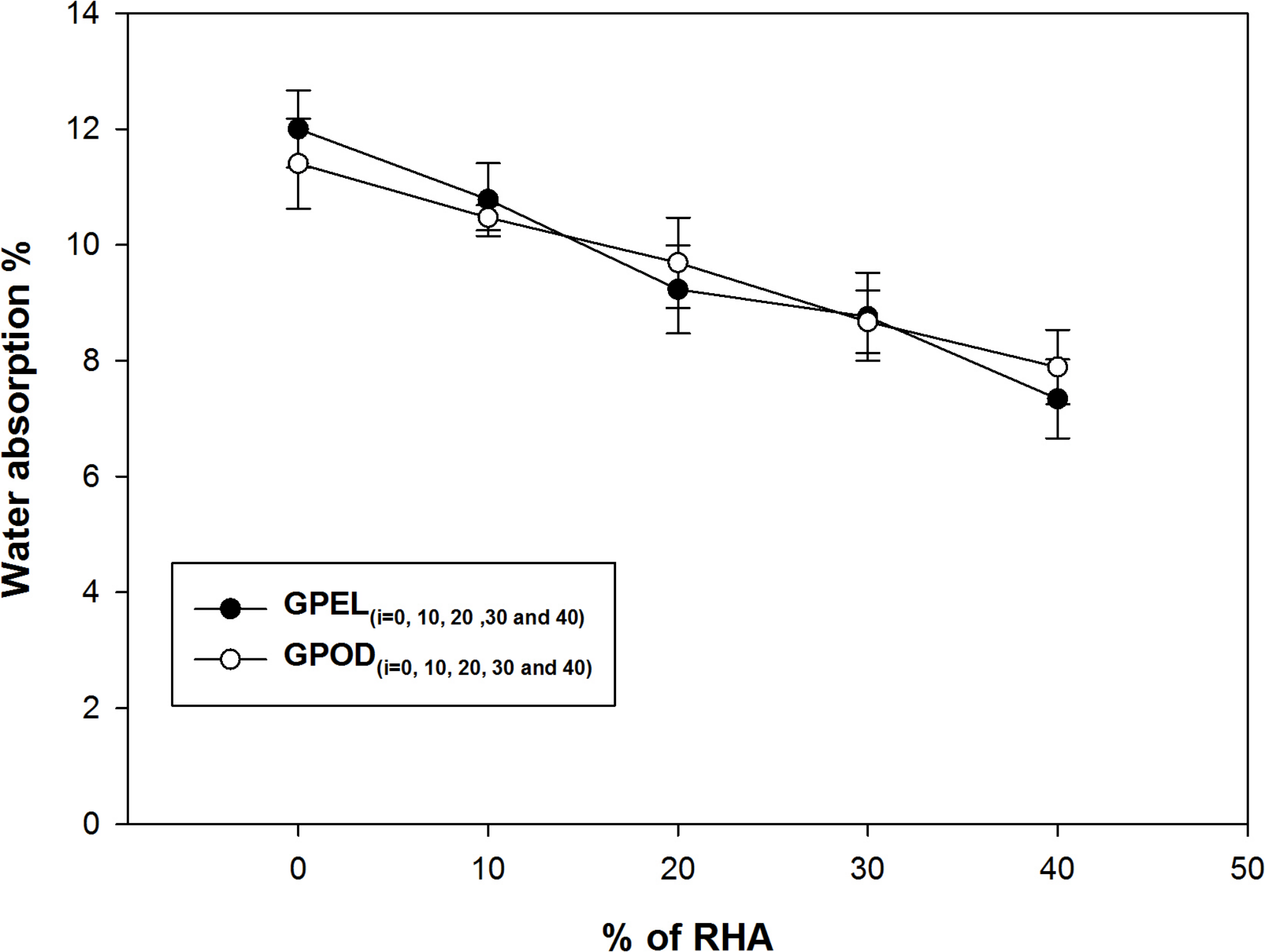
Water absorption %
% of RHA
0
2
4
6
8
10
12
14
0
10
20
30
40
50
GPEL(i=0, 10, 20 ,30 and 40)
GPOD(i=0, 10, 20, 30 and 40)

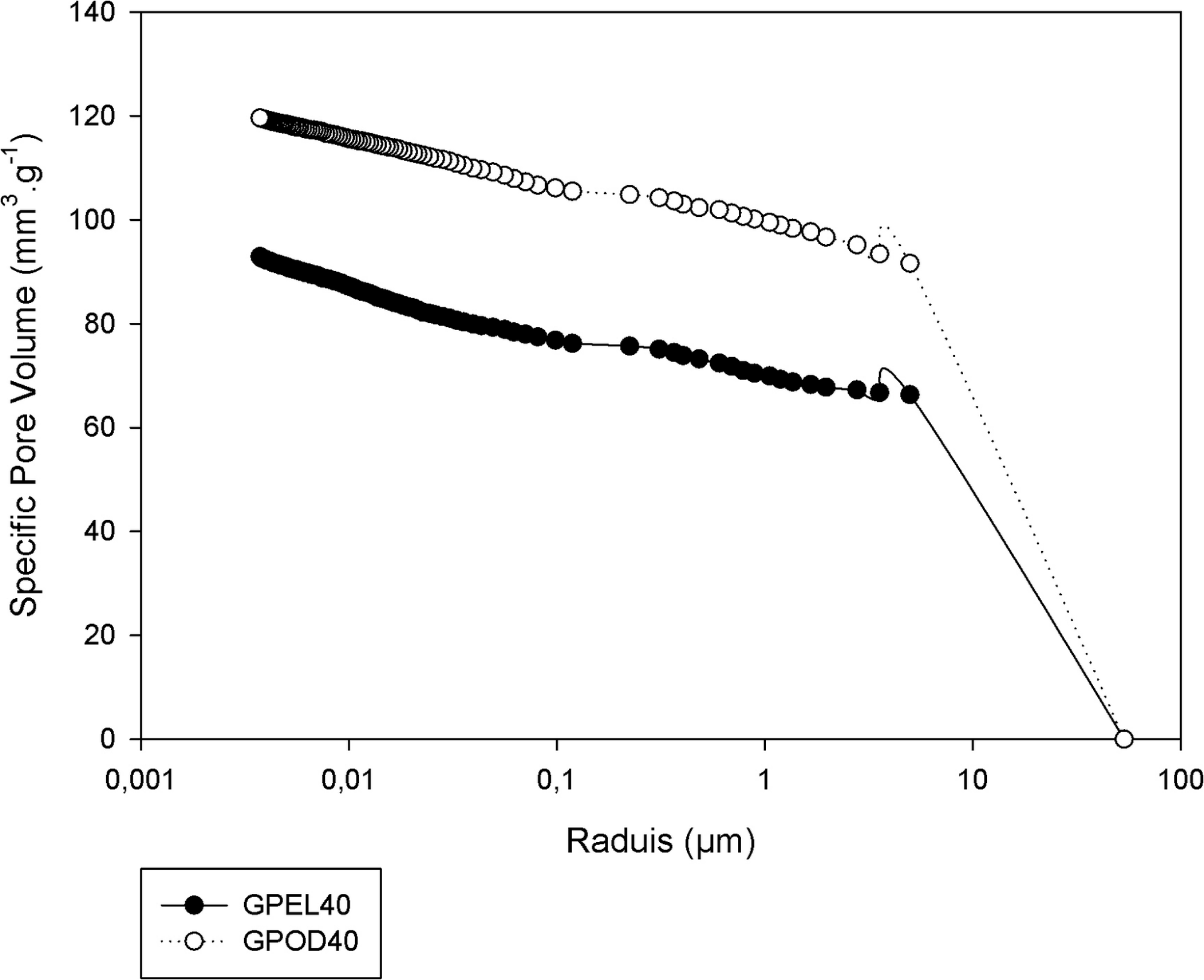
140
120
100
80
60
40
20
0
Specific Pore Volume (mm3.g-1)
0,001
0,01
0,1
1
10
100
Raduis (µm)
GPEL40
GPOD40

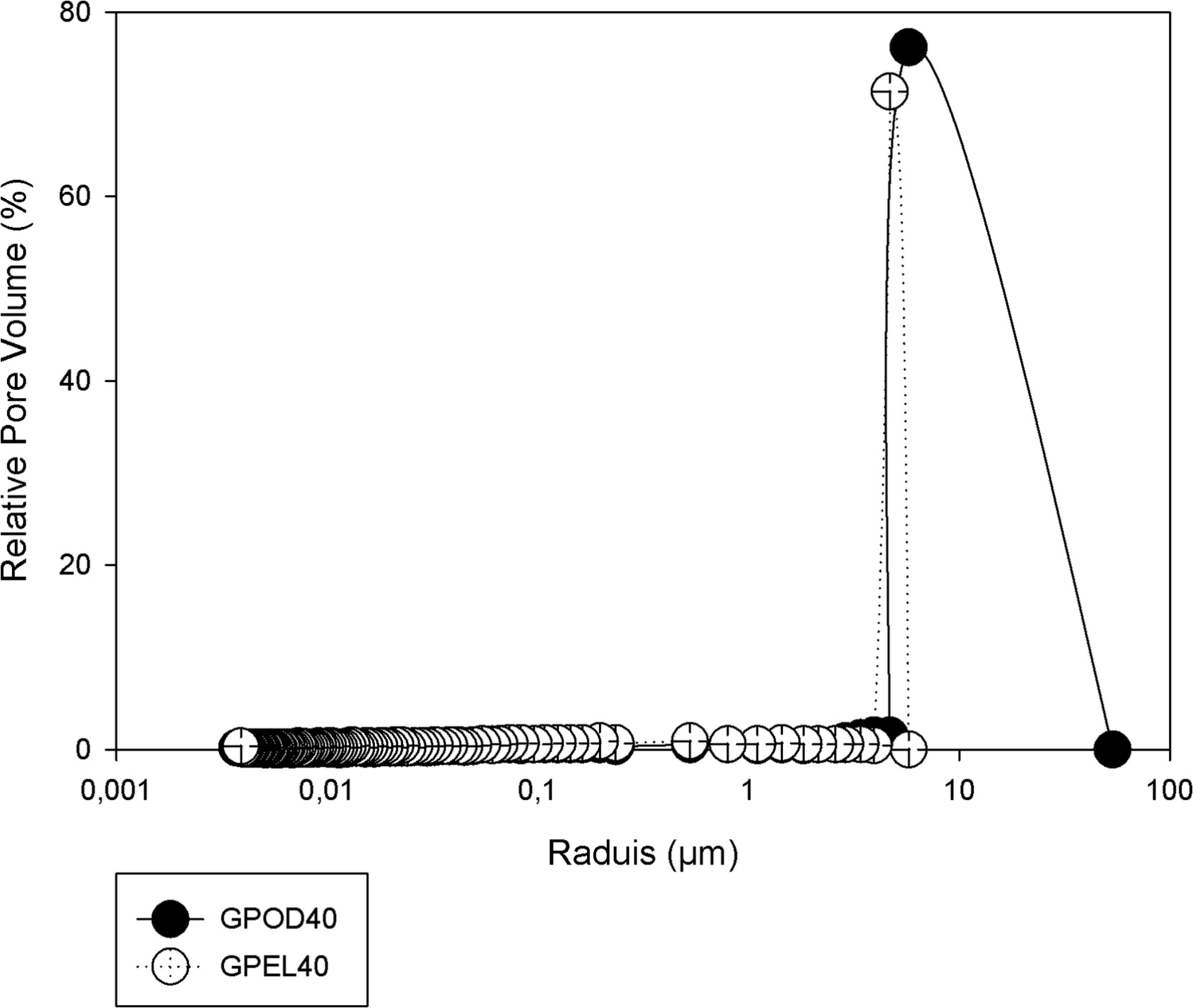
80
60
40
20
0
Relative Pore Volume (%)
0,001
0,01
0,1
1
10
100
Raduis (µm)
GPOD40
GPEL40

Table 1: Chemical compositions of raw materials

Oxides % wt.	Fe_2O_3	SiO_2	Al_2O_3	TiO_2	V_2O_5	P_2O_5	Cr_2O_3	K_2O	Na_2O	L.O.I
Laterite from Odza (OD)	37.5	25.1	23.0	0.908	0.150	0.148	0.227	-	-	12.7
Laterite from Eloumden (EL)	36.9	27.7	22.4	0.733	0.120	0.170	-	-	-	11.6
Rice husk ash (RHA)	0.196	93.89	0.584	0.033	-	0.498	-	3.045	0.083	1.2
River sand	0.69	98.03	0.43	0.90	-	-	-	0.26	0.31	9.12

Table 2: Particle sizes distribution and specific surface area of laterites.

Particle sizes (μm)	Laterite from Odza (OD)	Laterite from Eloumden (EL)
$d_{0.1}$	2.475	3.389
$d_{0.5}$	38.270	34.853
$d_{0.9}$	170.695	106.188
B.E.T surfaces (m^2/ g)	21. 92 ± 0.11	23.87 ± 0.13

Table 3: Design formulation of laterite-based geopolymer composites

Samples	Laterite (g)	Rice husk ash (RHA) (g)	River sand (g)	NaOH solution (8M) (g)	Sodium silicate (Na_2SiO_3) (g)
GPOD	100	0	200	45	45
GPOD10	90	10	200	45	45
GPOD20	80	20	200	45	45
GPOD30	70	30	200	45	45
GPOD40	60	40	200	45	45
GPEL	100	0	200	45	45
GPEL10	90	10	200	45	45
GPEL20	80	20	200	45	45
GPEL30	70	30	200	45	45
GPEL40	60	40	200	45	45